AFRL-IF-RS-TR-1999-188
Final Technical Report
September 1999

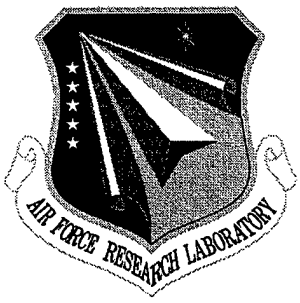

3-D HOLOGRAPHIC ROM

Holoplex, Inc.

Fai Mok

APPROVED FOR PUBLIC RELEASE; DISTRIBUTION UNLIMITED.

AIR FORCE RESEARCH LABORATORY
INFORMATION DIRECTORATE
ROME RESEARCH SITE
ROME, NEW YORK

This report has been reviewed by the Air Force Research Laboratory, Information Directorate, Public Affairs Office (IFOIPA) and is releasable to the National Technical Information Service (NTIS). At NTIS it will be releasable to the general public, including foreign nations.

AFRL-IF-RS-TR-1999-188 has been reviewed and is approved for publication.

APPROVED: Bernard J Clarke

BERNARD J. CLARKE
Project Engineer

FOR THE DIRECTOR: John V McNamara

JOHN V. MCNAMARA, Technical Advisor
Information & Intelligence Exploitation Division
Information Directorate

If your address has changed or if you wish to be removed from the Air Force Research Laboratory Rome Research Site mailing list, or if the addressee is no longer employed by your organization, please notify AFRL/IFED, 32 Brooks Rd, Rome, NY 13441-4114. This will assist us in maintaining a current mailing list.

Do not return copies of this report unless contractual obligations or notices on a specific document require that it be returned.

REPORT DOCUMENTATION PAGE	Form Approved OMB No. 0704-0188

1. AGENCY USE ONLY *(Leave blank)*	2. REPORT DATE	3. REPORT TYPE AND DATES COVERED
	Sep 99	Final Aug 95 - Feb 99

4. TITLE AND SUBTITLE

3-D HOLOGRAPHIC ROM

5. FUNDING NUMBERS

C - F30602-95-C-0125
PE - 62702F
PR - 4594
TA - 15
WU - P9

6. AUTHOR(S)

FAI MOK

7. PERFORMING ORGANIZATION NAME(S) AND ADDRESS(ES)

Holographic, Inc.
600 S. Lake St, Suite 102
Pasadena CA 91106

8. PERFORMING ORGANIZATION REPORT NUMBER

N/A

9. SPONSORING/MONITORING AGENCY NAME(S) AND ADDRESS(ES)

AFRL/IFED
32 Brooks Rd
Rome NY 13441-4114

10. SPONSORING/MONITORING AGENCY REPORT NUMBER

AFRL-IF-RS-TR-1999-188

11. SUPPLEMENTARY NOTES

AFRL Project Engineer: Bernard J. Clarke, IFED, 315-330-2106

12a. DISTRIBUTION AVAILABILITY STATEMENT

Approved for public release; distribution unlimited.

12b. DISTRIBUTION CODE

13. ABSTRACT *(Maximum 200 words)*

Holoplex has designed and constructed a 3-D holographic WORM disk system capable of stand-alone operation or used to produce master disks for mass-produced holographic ROM (HROM) systems. The storage capacity of the current system is 0.33 Tbits per 12 cm diameter disk. The recording rate is 240 Kbits/sec (a recording rate of 180 Mbits/sec was demonstrated using a more advanced setup.) The readout rate is 5.1 Mbits/sec using a single tap, large format CCD array. The surface density at any given spot on the disk is 42 bits/um2. This is achieved by multiplexing 84 holograms per location using a combination of peristrophic and angle multiplexing techniques. The entire setup was construed from readily available off-the-shelf components and a pair of custom designed imaging lenses.

14. SUBJECT TERMS

Optical Memory, Dye Polymer, Holographic Storage

15. NUMBER OF PAGES

44

16. PRICE CODE

17. SECURITY CLASSIFICATION OF REPORT	18. SECURITY CLASSIFICATION OF THIS PAGE	19. SECURITY CLASSIFICATION OF ABSTRACT	20. LIMITATION OF ABSTRACT
UNCLASSIFIED	UNCLASSIFIED	UNCLASSIFIED	UL

Table of Contents

1.0 Introduction

Holoplex has designed and constructed a 3-D holographic WORM disk system capable of stand-along operation or used to produce master disks for mass-produced holographic ROM (HROM) systems. The storage capacity of the current system is 0.35 Tbits per 12 cm diameter disk. The recording rate is 240 Kbits/sec (a recording rate of 180 Mbits/sec was demonstrated using a more advanced setup). The readout rate is 5.1 Mbits/sec using a single tap, large format CCD array. The surface density at any given spot on the disk is 42 bits/μm^2. This is achieved by multiplexing 84 holograms per location using a combination of peristrophic and angle multiplexing techniques. The entire setup was constructed from readily available off-the-shelf components and a pair of custom designed imaging lenses.

In this final report we document the work done characterizing the recording material (Section 2), the spatial light modulator (Section 3), building the high density recorder (Section 4), and the results of a system level demonstration (Section 5).

2.0 Storage Medium Characterization

DuPont has over 20 years of experience in manufacturing photopolymers for holography and currently produces a complete line of OMNIDEX™ films covering the wavelength range from 450 to 660 nm. The OMNIDEX™ films are completely self-processing and the holographic images form in real time. Since it is a commercial product, the final hologram has been tested at high temperatures with humidity and solar UV exposure without noticeable degradation in quality. Applications of these films include: holographic data storage, head-up-display in cars and planes, fiber optic demultiplexers, helmet mounted displays, holoarts, micro-optics, high resolution lithography, Fourier-plane matched filters for pattern recognition, etc.

The recipe for making DuPont's photopolymer is fairly simple and the ingredients include: solvents, polymeric binders, acrylic monomers, plasticizers, photosensitizing dyes, initiating systems, and chain transfer agents. These ingredients are mixed and then dissolved in the solvent. The polymeric binders serve to hold the goo together after it is cast onto 200D Mylar® polyester film using conventional web coaters and the solvents allowed to evaporate. A thin protective cover sheet (usually Mylar film) is then applied to the tacky coating for compete coverage. DuPont's photopolymer is shipped to the customer in rolled drums, page sized sheets, or in some instances, in the original solution form. The solution form is useful if the customer wants to cast or spin coat on his or her own substrates.

Figure 2.1 shows how illumination causes the index of the photopolymer to change. Two laser beams intersect in the photopolymer and setup a sinusoidal interference pattern. The photosensitizing dye absorbs the incident photons and triggers the photoinitiator system to begin photopolymerization of the acrylic monomers (several different photosensitizing dyes could be mixed in one photopolymer to achieve wide color sensitivity). The consumption of monomers in the bright region sets up a monomer concentration gradient, causing net diffusion of monomers from the dark into the bright regions. Polymerization and diffusion of the monomers continue until either the illumination source is removed, or all the monomers are used up. The local index variation in the photopolymer results from the increased density in the bright regions.

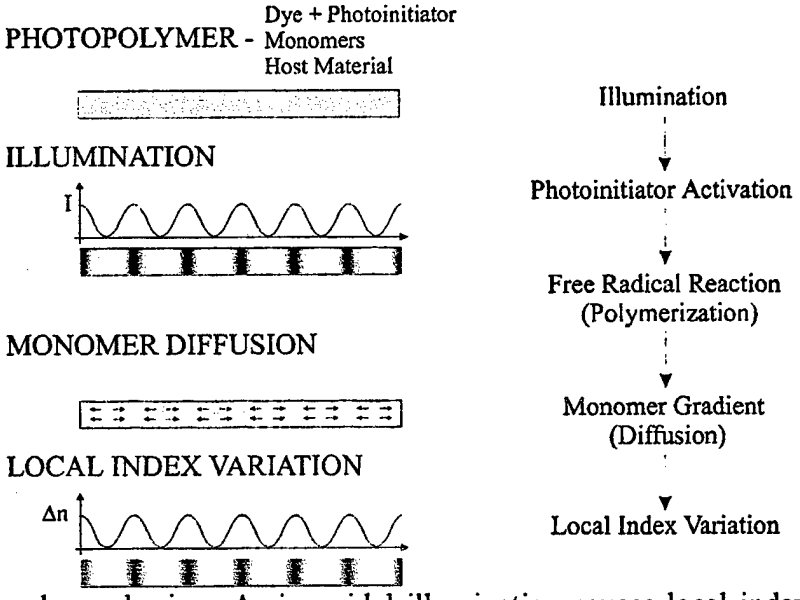

Figure 2.1: Photopolymer basics. A sinusoidal illumination causes local index variation in the photopolymer.

Three to four steps are usually involved in using the DuPont photopolymer for holography: (1) laminate or spin coat the photopolymer to a supporting substrate, (2) exposure to laser illumination in the proper wavelength range, (3) a uniform UV exposure to cure the material of excess monomers, (4) heating the cured photopolymer to increase index modulation. Step 4 is recommended for some DuPont photopolymer but is not required. The heat softens the film and allows further monomer diffusion. This can sometimes increase the index modulation by a factor of 2 to 3 times.

One problem with the OMNIDEX™ series photopolymer is their limited thickness of 10 to 25 μm. Unlike photorefractive crystals, the DuPont photopolymers cannot be polished because it is soft and tacky (before complete polymerization). Therefore, in order to maintain good optical quality, the film is made very thin. DuPont also produces an experimental-grade photopolymer in 38 and 100 micron thick versions (HRF-150-38 and HRF-150-100). They are sensitive to the blue-green wavelengths and behave similarly to the OMNIDEX™ films (except baking to increase the index modulation is not recommended with the HRF series). Since the number of holograms that can be multiplexed at a given location is directly proportional to the thickness of the recording material (therefore surface density and storage capacity as well), we use the DuPont HRF-150 100 microns thick photopolymer for the experiments.

Figure 2.2 shows the cumulative grating strength as a function of exposure energy for the HRF-150-100 material from DuPont tested at 532 nm. This curve was obtained by multiplexing 100 planewave holograms at a single location and then summing the square-root of the measured diffraction efficiency of the stored holograms sequentially as a function of the cumulative exposure energy the material had experienced. Figure 2.2 shows that the HRF-150-100 material requires about 35 mJ/cm^2 of sensitizing exposure energy before grating formation occurs. The cumulative grating strength then grows quasi-linearly with exposure energy until around 150 mJ/cm^2 where the slope decreases rapidly due to material saturation (the monomers are exhausted). The final cumulative grating strength at saturation is approximately equal to the *M/#* of the recording material. The *M/#* of a recording material varies depending on experimental conditions such as material thickness, absorption, recording geometry, and the ratio of reference to signal beam intensity. After the *M/#* of a material is measured for a particular setup, it can be used to predict the diffraction efficiency obtainable for the number of holograms to be multiplexed. The relationship is:

$$\eta = \left(\frac{M/\#}{M}\right)^2 \qquad \text{Eq. 2.1}$$

where η is the diffraction efficiency and M is the number of holograms to be multiplexed. The *M/#* for the DuPont HRF-150-100 material is around 6.5 (Figure 2.2 indicates a final cumulative grating strength of about 7 but we generally consider the material fully saturated by about 175 mJ/cm^2 of cumulative exposure). For example, if we were to multiplex 1,000 holograms in the HRF-150-100 photopolymer, Equation 2.1 would predict a diffraction efficiency of $(6.5/1{,}000)^2 = 4 \times 10^{-5}$ per hologram.

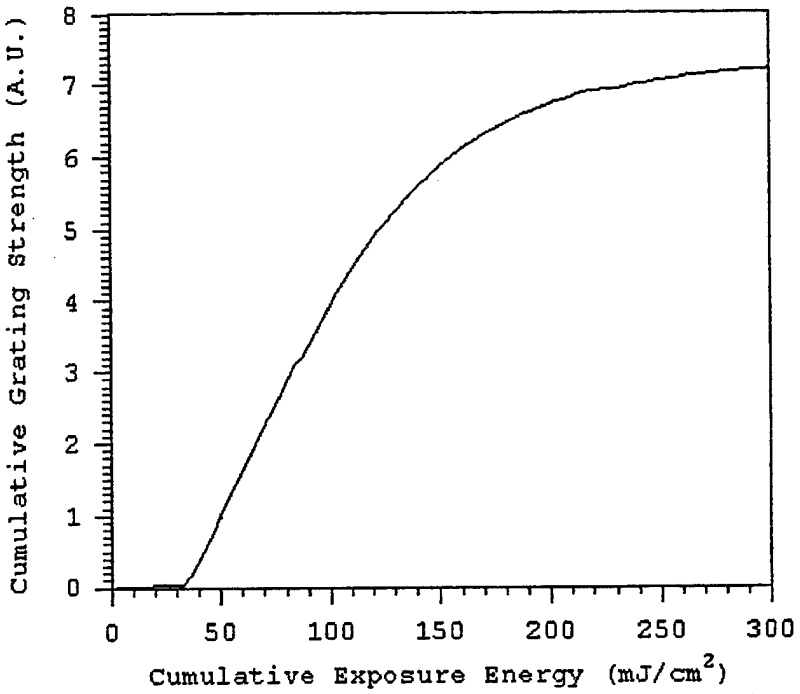

Figure 2.2: Cumulative grating strength as a function of exposure energy for the DuPont HRF-150 100 microns thick photopolymer.

Other than the dynamic range of the recording material, we are also interested in its optical quality. Due to the casting process in which the DuPont material is made, the surface shows visible dimples and thickness variations. Considerable scattering noise results from these non-uniformities but the more immediate and noticeable effect is on the image quality (the dimples and thickness variations distorts the data pattern imaged from the SLM, through the recording material, to the detector array). To quantify surface quality of various recording materials, we constructed an interferometer system shown in Figure 2.3.

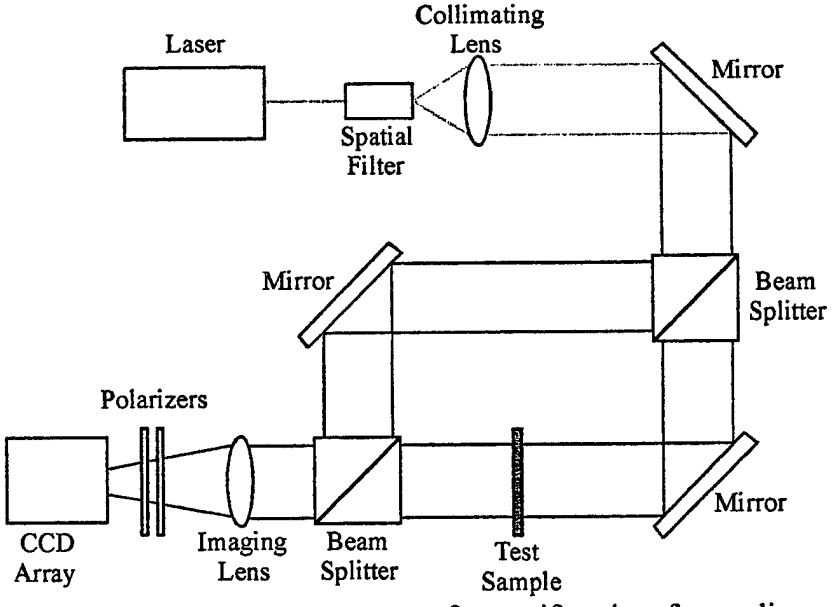

Figure 2.3: Interferometer system to test surface uniformity of recording materials..

The interferometer system shown in Figure 2.3 is fairly simple. The raw beam from a 532 nm DPSS (Diode Pumped Solid State) laser is expanded/collimated to form a uniform beam with a diameter of around 1 cm. The beam is then split and recombined using a pair of beam splitters and mirrors. The combined beam is then imaged through a pair of polarizers onto a CCD array so the intensity can be adjusted. The beam splitters and mirrors are aligned such that when no test sample is in the system, the CCD array sees an equally spaced interference pattern that is straight and parallel. Figure 2.4 shows the interference pattern generated when a 1 mm thick glass slide is placed in one arm of the interferometer. This glass slide is of the same type used to prepare the DuPont photopolymer for testing in the recorder (the DuPont photopolymer must be laminated on to a substrate for structural support). The interference pattern of Figure 2.4 is straight and parallel, indicating that the glass slide is of good optical quality.

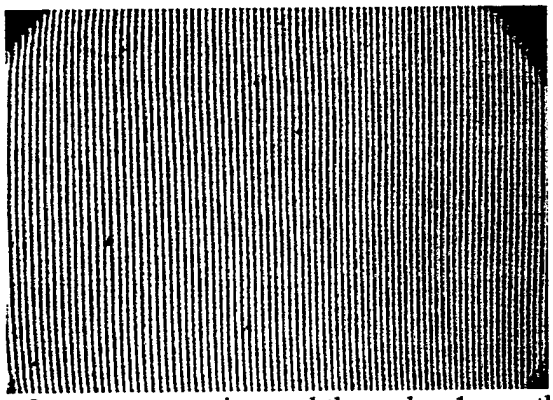

Figure 2.4: Interference pattern imaged through a 1 mm thick glass slide

Figure 2.5 shows the interference pattern generated when a 1 mm thick glass slide laminated with the 100 micron DuPont photopolymer is placed in one arm of the interferometer. The sample was cured with UV light to completely polymerize the photopolymer before testing. The resulting interference pattern instead of being straight and parallel, is wiggly and the period varies randomly across the field. The varying period indicates that the thickness of the laminated photopolymer changes and the wiggly lines show that there are localized deformities. Both of these non-uniformities degrade the SNR of the holograms by reducing pixel registration accuracy on the detector array and scatter light from bright pixels into the dark pixels.

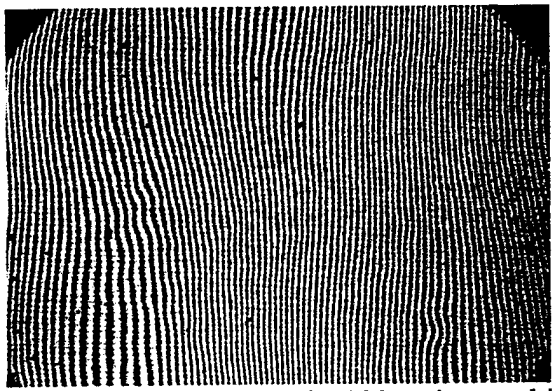

Figure 2.5: Interference pattern imaged through 100 micron thick DuPont photopolymer laminated on a 1 mm thick glass slide.

To properly quantify the imaging quality of the recording material under real conditions, we modified the high density recorder setup to image a chrome-on-glass mask through the recording material onto a 1-to-1 matched CCD array (Figure 2.6). The setup consists of a 50 mW laser source at 532 nm split with a polarized beam splitter to form the signal and reference arms. The numerous half-wave plates and polarizers surrounding the polarized beam splitter allows us to transfer power between the two arms. This configuration also allows the power in each arm to be adjusted without affecting the power in the other arm. The reference and signal raw beams are then expanded and collimated with separate systems so that only the necessary magnification is used in each arm to conserve power. Furthermore, any fix pattern noise from the beam splitter is filtered in the expansion process. In the signal beam, a chrome-on-glass mask with 24 um×24 um pixel pitch modulates the incident light and the pattern is imaged to the detector plane with a pair of custom designed f/1.1 lenses. A large format CCD array that has the same pixel pitch as the chrome mask is placed at the detector plane. The mask – f/1.1 lenses – CCD array combination is carefully aligned to obtain pixel matching between the mask and CCD array across the entire field-of-view of the f/1.1 lenses. The test sample, DuPont's HRF-150 100 microns thick photopolymer laminated on a 1 mm thick glass, is mounted on a custom designed rotational stage and placed slightly past the Fourier plane of the f/1.1 lenses. The rotational stage allows the recording material to be rotated in-plane to attain peristrophic multiplexing. The recording material is on-axis with respect to the signal beam (the plane of the recording material is perpendicular to the center ray of the signal beam). The field-of-view (FOV) of the custom designed f/1.1 lenses is 480 chrome mask pixels across at their largest diameter, capturing a total of 180,000 pixels (or bits) per hologram.

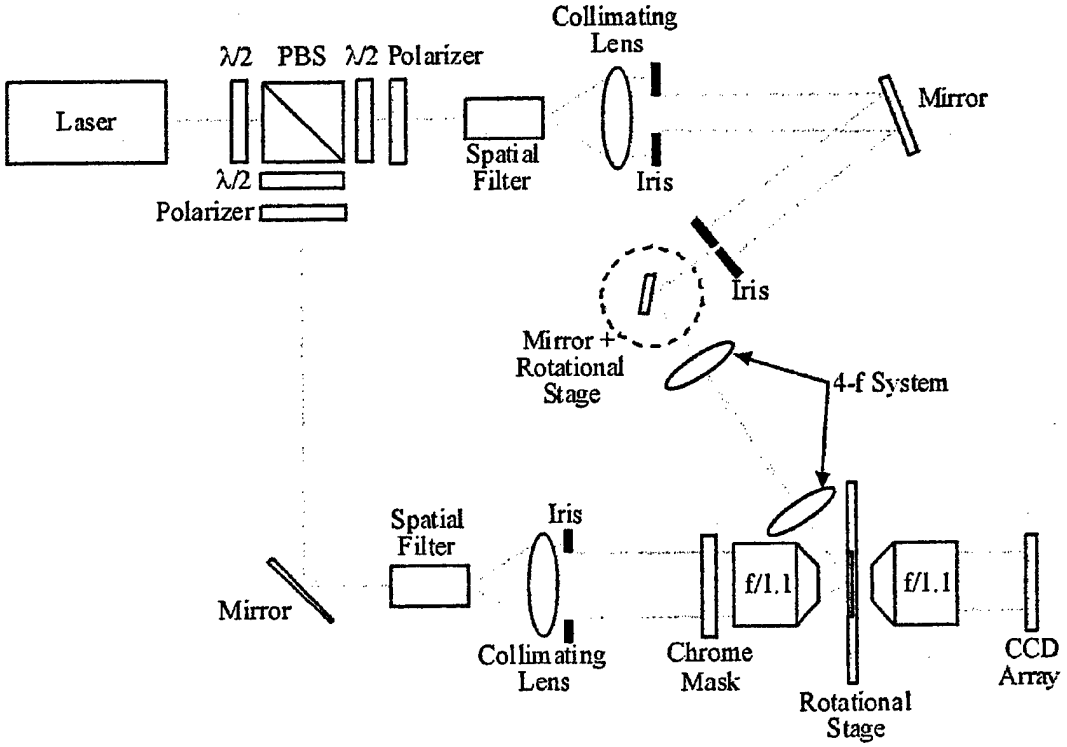

Figure 2.6: Modified high density recorder setup to characterize recording material imaging quality.

In the reference arm, the beam turns a corner and then deflects off of a mirror mounted on a computer controlled rotational stage. The deflected beam is then imaged onto the recording material with a pair of lenses in the 4-f geometry. This combination allows the incident angle of the reference beam on the recording material to change (by scanning the computer controlled rotational stage) without moving the illuminated area. In this particular setup, the range of angle in which the reference beam can be scanned without too much distortion is approximately 23 degrees. The resolution of the computer controlled rotational stage is 0.001° and the nominal incident angle of the reference beam with respect to the signal beam is 60°.

Figure 2.7 shows a partial image of what the data pattern on the chrome mask looks like (obtained by imaging the chrome mask onto the CCD array through the test sample). The data is arranged in 32×32 pixel blocks and the blocks are delineated with tracking marks for pixel matching purposes. The signal-to-noise-ratio (SNR) of representative blocks can be computed for comparison purposes. In computing the SNR, we assume the distribution of the bright (on) and dark (off) pixels are Gaussian so we can use Equation 2.2.

$$SNR = \frac{\mu_b - \mu_d}{\sqrt{\sigma_b^{\,2} + \sigma_d^{\,2}}} \qquad \text{Eq. 2.2}$$

where μ_b, μ_d, σ_b^2, σ_d^2 are the mean of the bright pixels, mean of the dark pixels, variance of the bright pixels, and the variance of the dark pixels, respectively. For the representative block shown in Figure 2.7, μ_b=186, μ_d=22, σ_b^2=231, σ_d^2=51, and the SNR=9.8. For comparison, a SNR of 11.1 was obtained when no test sample was placed between the imaging lenses. The small drop in SNR indicates that the DuPont material distorts the imaging condition slightly.

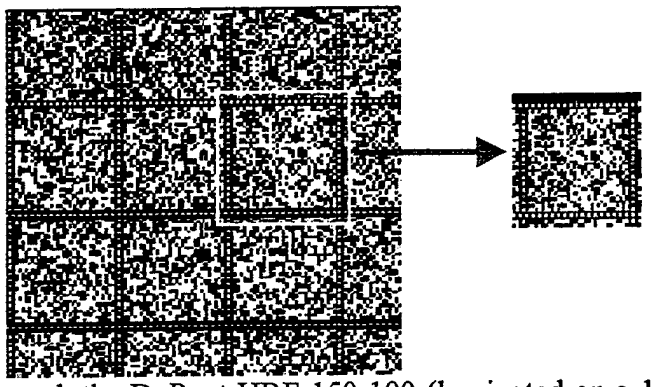

Figure 2.7: Imaging through the DuPont HRF-150-100 (laminated on a 1 mm thick glass slide) sample.

3.0 Spatial Light Modulator (SLM) Characterization

The spatial light modulator (SLM) we use in the construction of the high density recorder is a 640×480 pixels, active-matrix liquid crystal display from Kopin Corp. Its small size and low power requirement are well suited for the WORM system. For integration into the recorder, the Kopin SLM was anti-reflection coated on both sides by an outside vendor to reduce reflections and scattering noise. We also designed a random phase mask/lenslet array to mount in front of the SLM. This random phase mask reduces the intensity of the DC spot in the Fourier plane (which is really close to the plane of the recording material) so that the intensity of the signal beam on the recording material is more uniform. The lenslet array increases the total optical throughput of the SLM by focusing the available light through the switching area of the pixels. The random phase mask/lenslet array was fabricated and mounted by Jet Propulsion Laboratory of Pasadena.

Figure 3.1 shows a blow up image of what a 2×2 checkerboard pattern looks like on the Kopin SLM. This picture was obtained by illuminating the SLM (without the random phase mask /lenslet array) with a uniform planewave and then imaged with a lens onto a CCD array. One thing you notice right away is that the switching area of each pixel is fairly small and it doesn't have a regular rectangular shape. By eye it looks like the switching area of each pixel is only about 30% of the entire 24 um×24 um pixel size. Within the switching area, it is not all transmissive but contains a periodic bar shape.

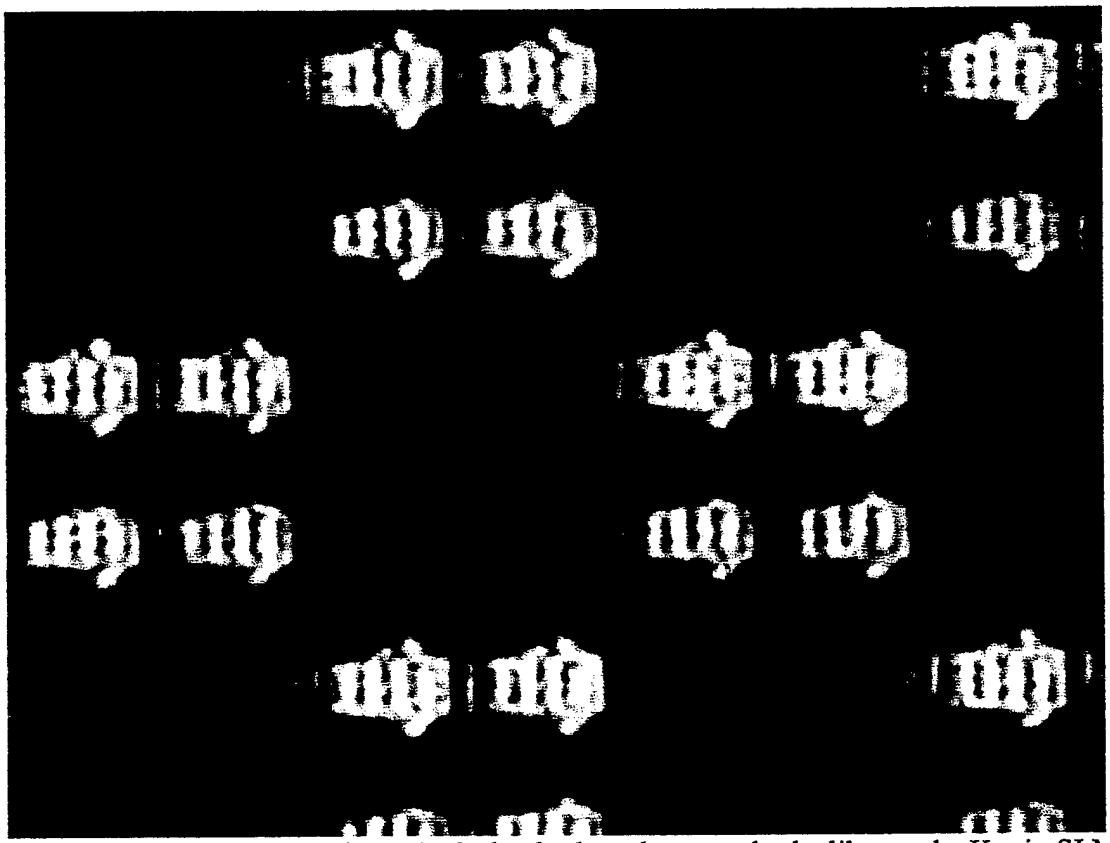

Figure 3.1: Blow up image of what a 2×2 checkerboard pattern looks like on the Kopin SLM.

One important parameter of spatial light modulators is the contrast ratio between bright (on) and dark (off) pixels. The contrast ratio of the SLM sets the upper limit on the SNR of a hologram. For the Kopin SLM, the contrast ratio between the on and off pixels depends on the modulation transfer function of the driving signal (the spatial frequency of the displayed image). Figure 3.2 shows the intensity of the pixel as a function of the pixel number (the consecutive pixels from left to right) for three different drive signals. For the red curve in Figure 3.2, the Kopin SLM is displaying a 4 pixels by 4 pixels checkerboard pattern and the best contrast ratio is more than 10:1. The green curve is for a 2×2 checkerboard pattern and the best contrast ratio drops to about 6:1. Finally when the highest spatial frequency is displayed on the Kopin SLM (1×1 checkerboard), the contrast ratio drops to as low as 2:1 as shown by the blue curve. We suspect this drop in contrast ratio when the spatial frequency is increased is due to the limited capability of the thin film transistors in the pixel to drive the capacitors in the switching area of the pixel fast enough. To confirm this suspicion we also measured the drive voltage going into the LCD panel to make sure the drop in contrast ratio is not due to the separate control electronics feeding the panel. Figure 3.3 (a) shows the drive voltage for a 1×1 checkerboard while Figure 3.3 (b) shows the drive voltage for a 2×2 checkerboard. The two figures show the same peak amplitude which indicate that the control electronics is supplying the same voltage regardless of spatial frequency.

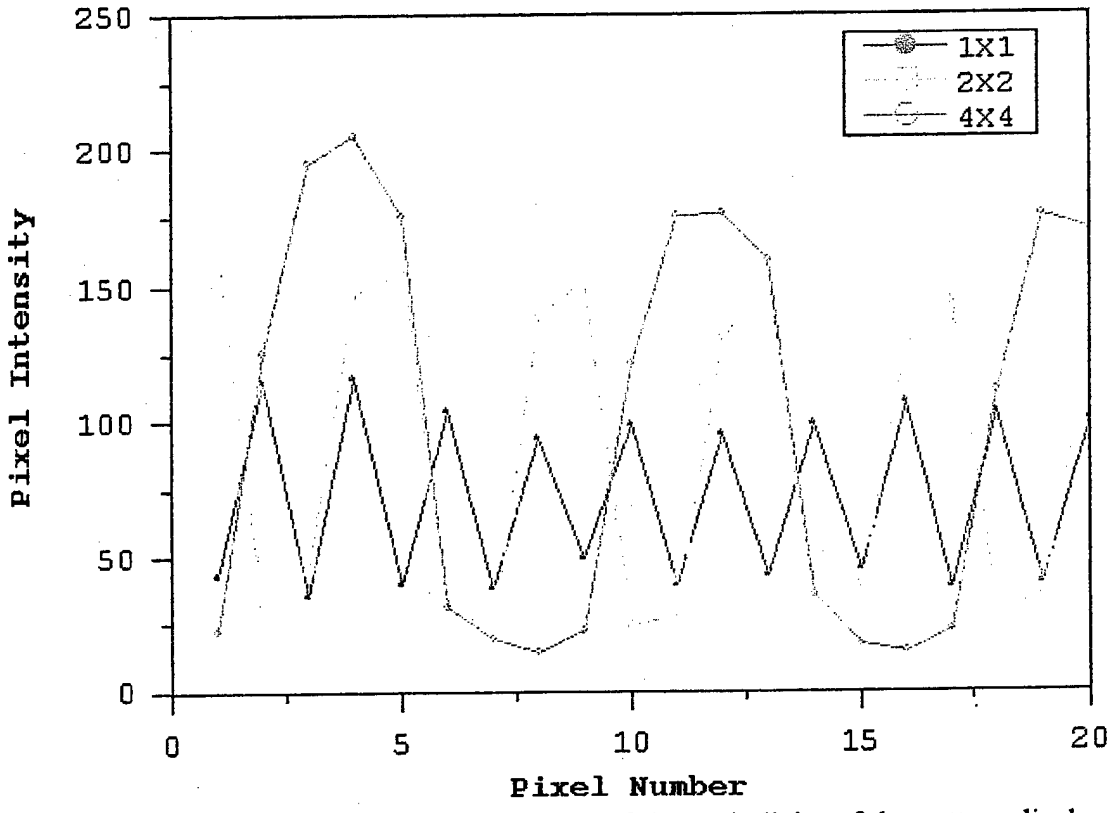

Figure 3.2: The intensity of the pixels as a function of the periodicity of the pattern displayed on the Kopin SLM.

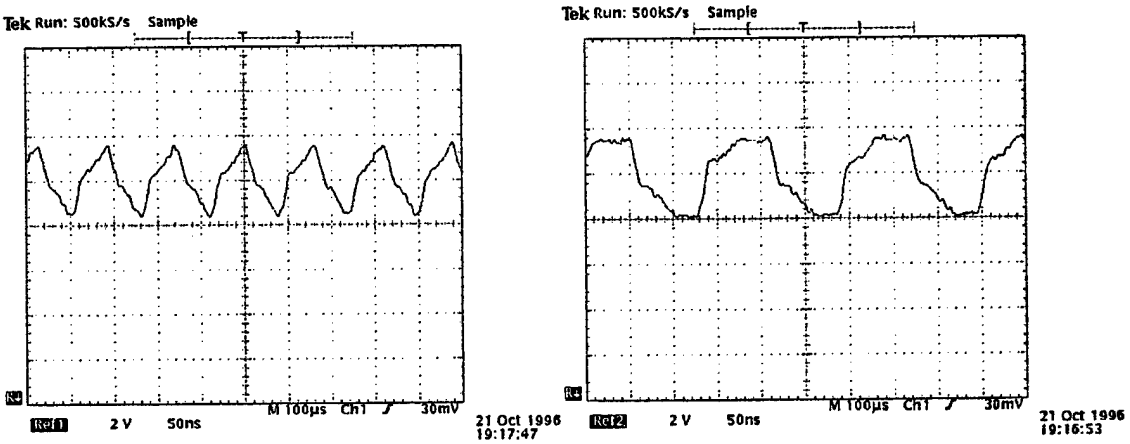

(a) (b)

Figure 3.3: The electrical drive signal for the (a) 1×1 and (b) 2×2 patterns taken from the Kopin SLM control circuitry (the control circuitry is separate from the LCD panel).

As stated above, the switching area of the Kopin SLM occupies only about 30% the real estate of each pixel. This means up to 70% of the light falling on the LCD panel does not contribute to the formation of the data page. Figure 3.4 shows an atomic force microscope picture of the random phase mask/lenslet array we designed and fabricated to help increase the throughput of the SLM. The random phase mask/lenslet array contains 640 by 480 pixels that are 1-to-1 matched to the Kopin SLM. Each pixel contains a convex surface like a lens and sits on a mesa that has one of four discrete heights from 0 to $\pi/2$. The 4 possible heights of the mesa are randomly distributed amongst the 640 by 480 pixels to create the random phase mask.

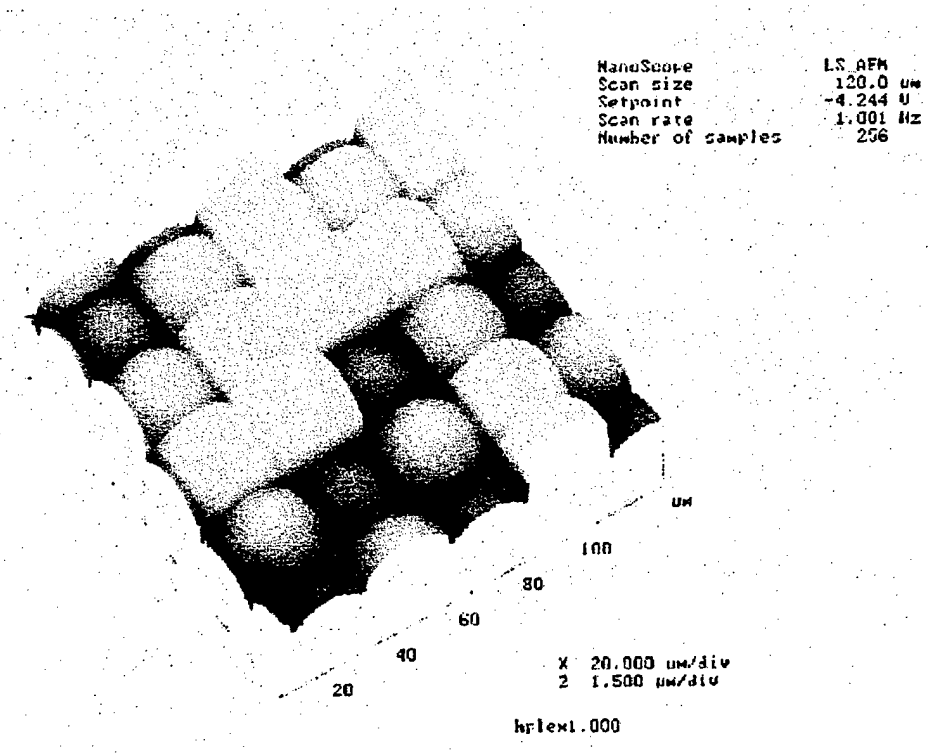

Figure 3.4: Atomic force microscope picture of the micro-lens array.

Figure 3.5 shows four images obtained by illuminating the random phase mask/lenslet array from one side with a uniform planewave and placing a CCD array on the other side. Figure 3.5 (a) shows the image obtained with the CCD array really close to the random phase mask/lenslet array before the planewave had come to a focus. Figure 3.5 (b) shows the image obtained with the CCD array exactly at the focal plane of the lenslet array. The planewave comes to a sharp focus and when mounted to the SLM, this focal point should be directly on the switching area of the SLM for maximum throughput. Figure 3.5 (c) shows the image obtained with the CCD array slightly past the focal point. The light at this point is fairly spread out. Figure 3.5 (d) shows the image obtained with the CCD array far past the focal point. Now all that is visible is the structure of the pixels outlined by the different depth of the random phase mask.

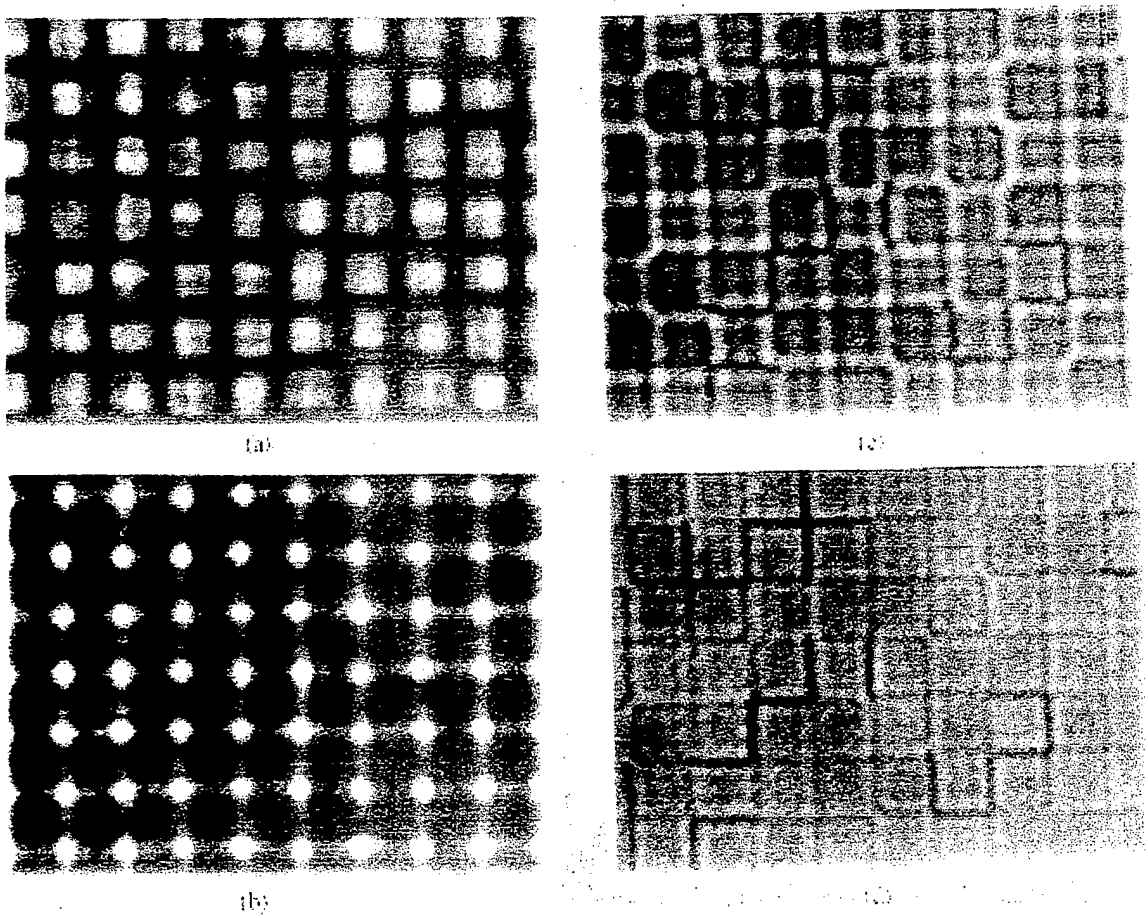

Figure 3.5: The CCD array at (a) the near side of the focal plane; (b) the focal plane; (c) the far side of the focal plane; (d) far-far side of the focal plane.

The random phase mask/lenslet array was carefully aligned and mounted on a Kopin SLM with optical glue by Jet Propulsion Laboratory (JPL) of Pasadena. Unfortunately, the finished product had visible "Newton Rings" which affected the uniformity of the data page across the SLM. We suspect the mounting of the random phase mask/lenslet array introduced some stress on the Kopin SLM, causing the "Newton Rings" effect. Until the "Newton Rings" is

resolved, we will continue the experiments using the standard Kopin SLM. Figure 3.6 shows a picture of the Kopin SLM with the random phase mask/lenslet array mounted.

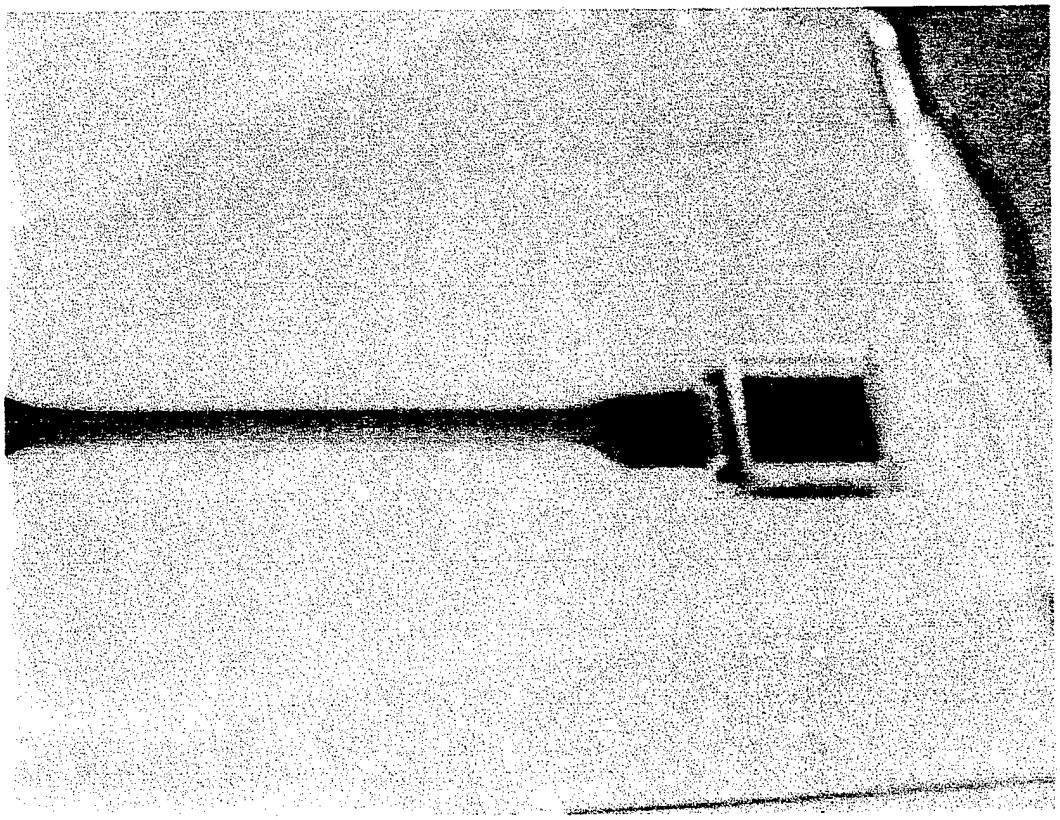

Figure 3.6: A picture of the Kopin SLM with the random phase mask/lenslet array mounted on top.

Recently, a new type of display device called the Digital Mirror Device (DMD) became available from Texas Instrument. We procured one such device in the form of a presentation projector and took it apart to get to the DMD chip and drive circuitry. This device has 800×600 pixels, each pixel is a micro-mirror capable of deflecting incident light to one of two possible angles. Thus the DMD is inherently a binary device so the contrast ratio should be very good. For use as a presentation projector, a color wheel is placed in the beam path to produce color. Gray-levels are obtained by switching the micro-mirrors with a duty cycle. Figure 3.7 shows a functional diagram of the DMD device. A collimated white light source incident normally on the DMD chip. The micro-mirrors representing the pixels can tilt either +10 or –10 degrees from the normal direction of the DMD plane. Therefore the two possible reflected beams are ± 20 degrees from the normal as shown in Figure 3.7. We can pick one of the directions as 'on' pixels and the other as 'off'. In the 'on' path are the color wheels and imaging lenses while the 'off' path is absorbed.

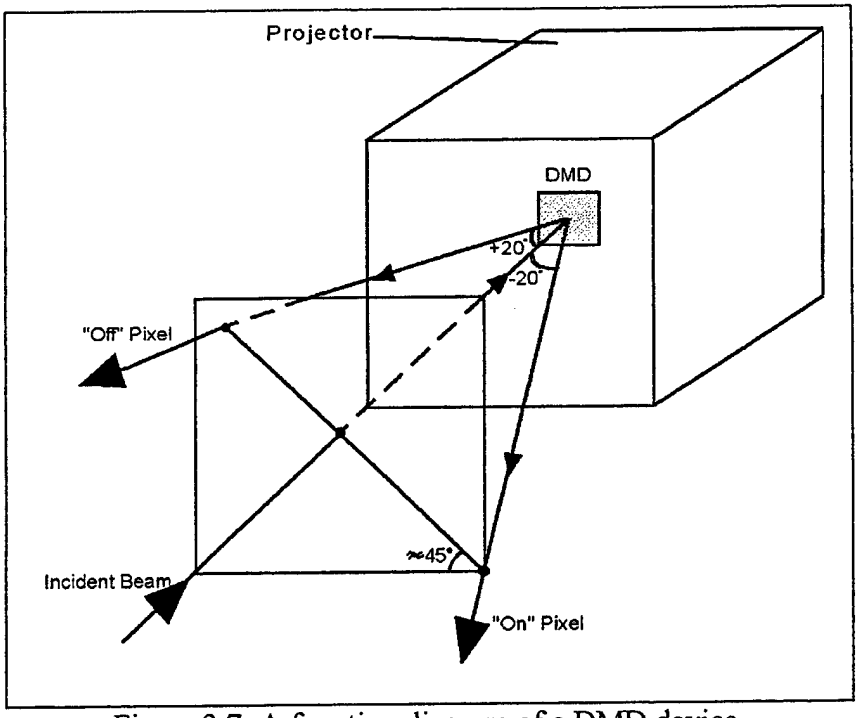

Figure 3.7: A function diagram of a DMD device.

We have measured the optical properties of the DMD device for comparison with the Kopin. Figure 3.8 shows a blow up image of what a 2×2 checkerboard pattern looks like on the DMD device. This picture was obtained by illuminating the DMD normally with a uniform planewave and then imaging the 'on' path with a lens onto a CCD array. Comparing with the Kopin SLM, the switching area of the DMD is quite large (each white square in Figure 3.8 is actually composed of 4 micro-mirrors). The black dot at the center of each pixel is actually a hinge holding the micro-mirror in place.

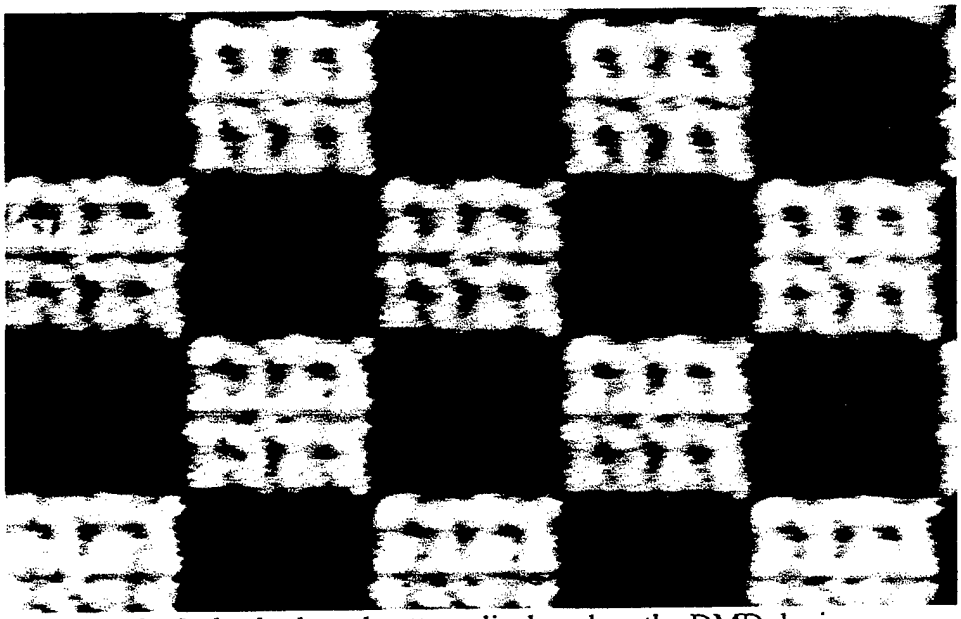
Figure 3.8: A 2×2 checkerboard pattern displayed on the DMD device.

We also displayed different spatial frequency images on the DMD device and found the contrast ratio to be fairly constant as shown in Figure 3.9. The observed contrast ratio was better than 200:1 and the measurement was limited by the 8-bits resolution of the frame grabber used.

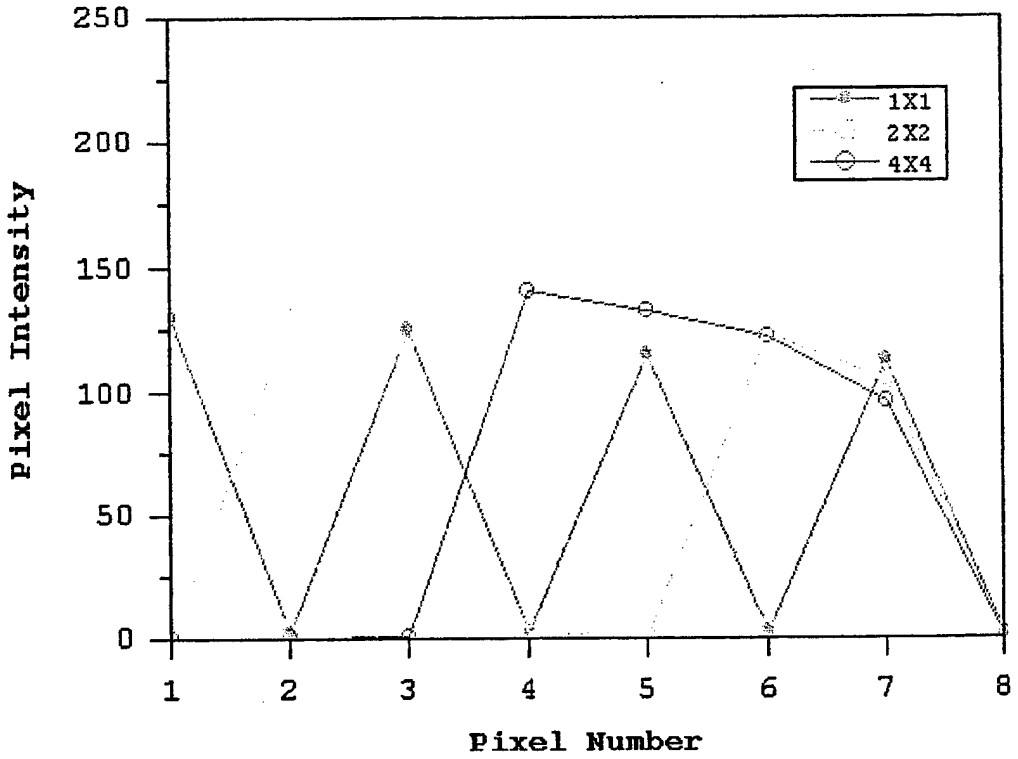

Figure 3.9: The intensity of the pixels as a function of the spatial frequency of the pattern displayed on the DMD device.

Initial tests indicate that the DMD device outperforms the Kopin SLM in both the contrast ratio and optical throughput. It seems that we should replace the Kopin SLM with the DMD device in the high density recorder setup immediately. However, a few details are stopping us from doing just that. First, the DMD device operates in the reflection mode while the Kopin SLM operates in the transmission mode. Considerable redesign would have to be implemented to use the DMD device in the high density recorder. Furthermore, the small deflection angle of the micro-mirrors makes it difficult to use large numerical aperture lenses (for example the custom designed f/1.1 lenses) to image the DMD to the detector array (the lens will have to be so close to the DMD chip that the illuminating beam would be blocked). One approach to circumvent this problem is to send both the illuminating beam and the diffracted signal beam through the same lens. This will require a different special lens design. Another problem with the DMD device is its 17 um×17 um pixel pitch. If a non magnifying 1-to-1 imaging system is used to image the data page to the detector array, then the detector array must also have 17 um×17 um pixel pitch. We have not been able to find any 17 um×17 um pixel pitch CCD array thus far. Two possible ways of dealing with this are: (1) redesign the imaging lenses to get 1-1 imaging through some magnification or reduction; (2) design our own detector sensors using CMOS technology. We are considering both options.

4.0 High Density Holographic Storage

To test multiplexing scheme based on angle and peristrophic multiplexing, a high density recorder setup using a combination of commercially available and custom designed components was constructed. Figure 4.1 shows a schematic diagram of the setup. A 50 mW laser source at 532 nm is split with a polarized beam splitter to form the signal and reference arms. The numerous half-wave plates and polarizers surrounding the polarized beam splitter allows us to transfer power between the two arms. This configuration also allows the power in each arm to be adjusted without affecting the power in the other arm. The reference and signal raw beams are then expanded and collimated with separate systems so that only the necessary magnification is used in each arm to conserve power. Furthermore, any fix pattern noise from the beam splitter is filtered in the expansion process. In the signal beam, a KOPIN spatial-light-modulator (SLM) modulates the incident light and the data pattern is imaged to the detector plane with a pair of custom designed f/1.1 lenses. A large format CCD array that has the same pixel pitch as the KOPIN SLM is placed at the detector plane. The SLM – f/1.1 lenses – CCD array combination is carefully aligned to obtain pixel matching between the SLM and CCD array across the entire field-of-view of the f/1.1 lenses. The recording material, DuPont's HRF-150 100 microns thick photopolymer, is mounted on a custom designed rotational stage and placed slightly past the Fourier plane of the f/1.1 lenses. The rotational stage allows the recording material to be rotated in-plane to attain peristrophic multiplexing. The recording material is on-axis with respect to the signal beam (the plane of the recording material is perpendicular to the center ray of the signal beam).

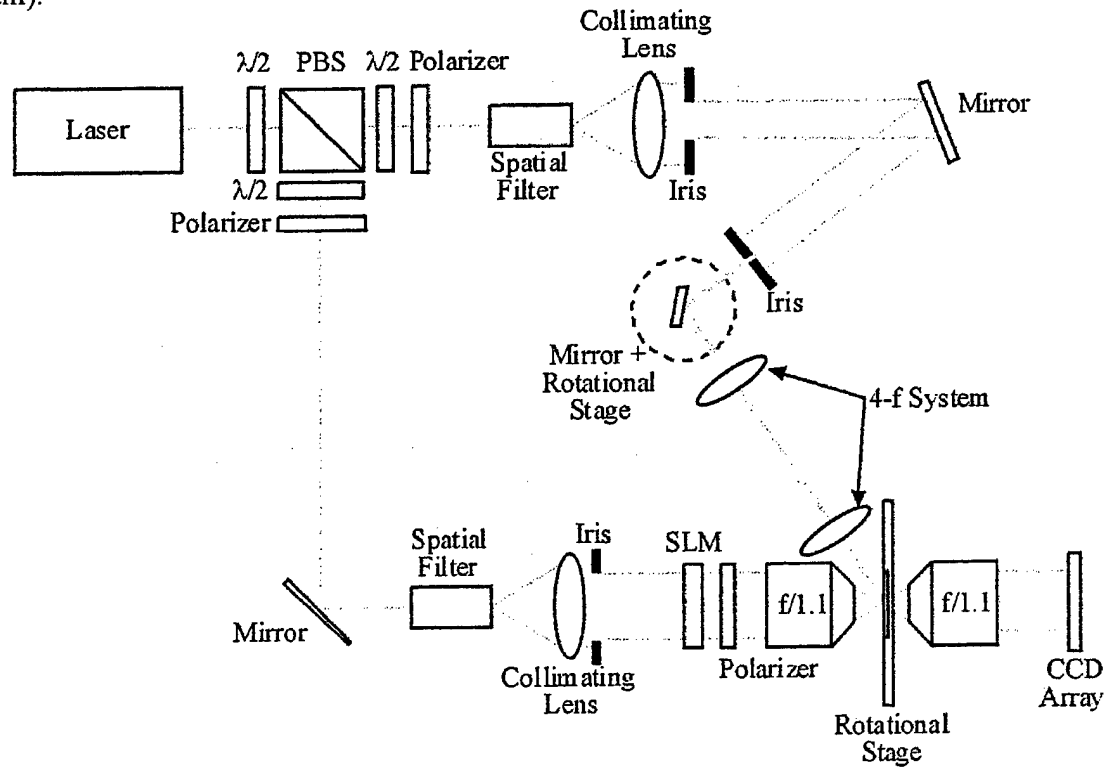

Figure 4.1: Experimental high density recorder setup using angle and peristrophic multiplexing.

In the reference arm, the beam turns a corner and then deflects off of a mirror mounted on a computer controlled rotational stage. The deflected beam is then imaged onto the recording material with a pair of lenses in the 4-f geometry. This combination allows the incident angle of the reference beam on the recording material to change (by scanning the computer controlled rotational stage) without moving the illuminated area. In this particular setup, the range of angle in which the reference beam can be scanned without too much distortion is approximately 23 degrees. The resolution of the computer controlled rotational stage is 0.001° and the nominal incident angle of the reference beam with respect to the signal beam is 60°.

The field-of-view (FOV) of the custom designed f/1.1 lenses is 480 KOPIN SLM pixels across at their largest diameter, capturing a total of 180,000 pixels (or bits) per hologram. The area of the hologram on the recording material is approximately 3.3×10^{-7} m^2. Therefore the surface density per hologram is 180,000 bits / 3.3×10^{-7} m^2, or 0.5 bits/μm^2. By multiplexing 80 holograms at a single location, we can achieve the surface density goal of 40 bits/μm^2.

Figure 4.2 shows an image of what a data pattern looks like (obtained by imaging the SLM onto the CCD array with a piece of 1 mm thick glass replacing the recording material). The data is arranged in 32×32 pixel blocks and the blocks are delineated with tracking marks for pixel matching purposes. The SNR is computed at five different regions to show the uniformity of the system. In computing the SNR, we assume the distribution of the bright (on) and dark (off) pixels are Gaussian so we could use Equation 2.2. For the center region, μ_b=203, μ_d=55, σ_b^2=412, σ_d^2=103, and the SNR=6.5. The relative uniformity of the SNR in the different regions of Figure 2 indicates: (1) the SLM pixels are aligned with the CCD array across the entire FOV of the f/1.1 lenses, (2) the intensity of the signal beam is fairly uniform across the FOV of the f/1.1 lenses, (3) our custom designed f/1.1 lenses have low distortion near the edge of the lenses.

Figure 4.3 shows the reconstructed data pattern from a single hologram stored in the DuPont material. The hologram was stored with a 0.5 second exposure and then UV cured to burn off the remaining dynamic range. Due to material shrinkage during the curing stage, the reference beam had to be de-tuned by 1.3° in order to re-Bragg match the largest possible portion of the data pattern. The shrinkage effect produces a non-uniform intensity profile that is very noticeable in Figure 4.3. The upper, middle, and lower sections lie along a line that is orthogonal to the plane of interaction (the plane formed by the center ray of the reference and signal beams). Therefore, they are largely unaffected by material shrinkage when the reference beam is de-tuned to Bragg match the middle section. However, the right and left sections are along the plane of interaction so they suffer some distortion and Bragg mis-match when the reference beam is de-tuned to Bragg match the middle section. Distortion causes a mismatch between the reconstructed data pixels and the detector pixels. Bragg mis-match lowers the intensity of the reconstructed pixels. Therefore the intensity and the SNR at the left and right regions are significantly lower than those of Figure 4.2 (the SNR at the left region was not computable due to the extremely low intensity).

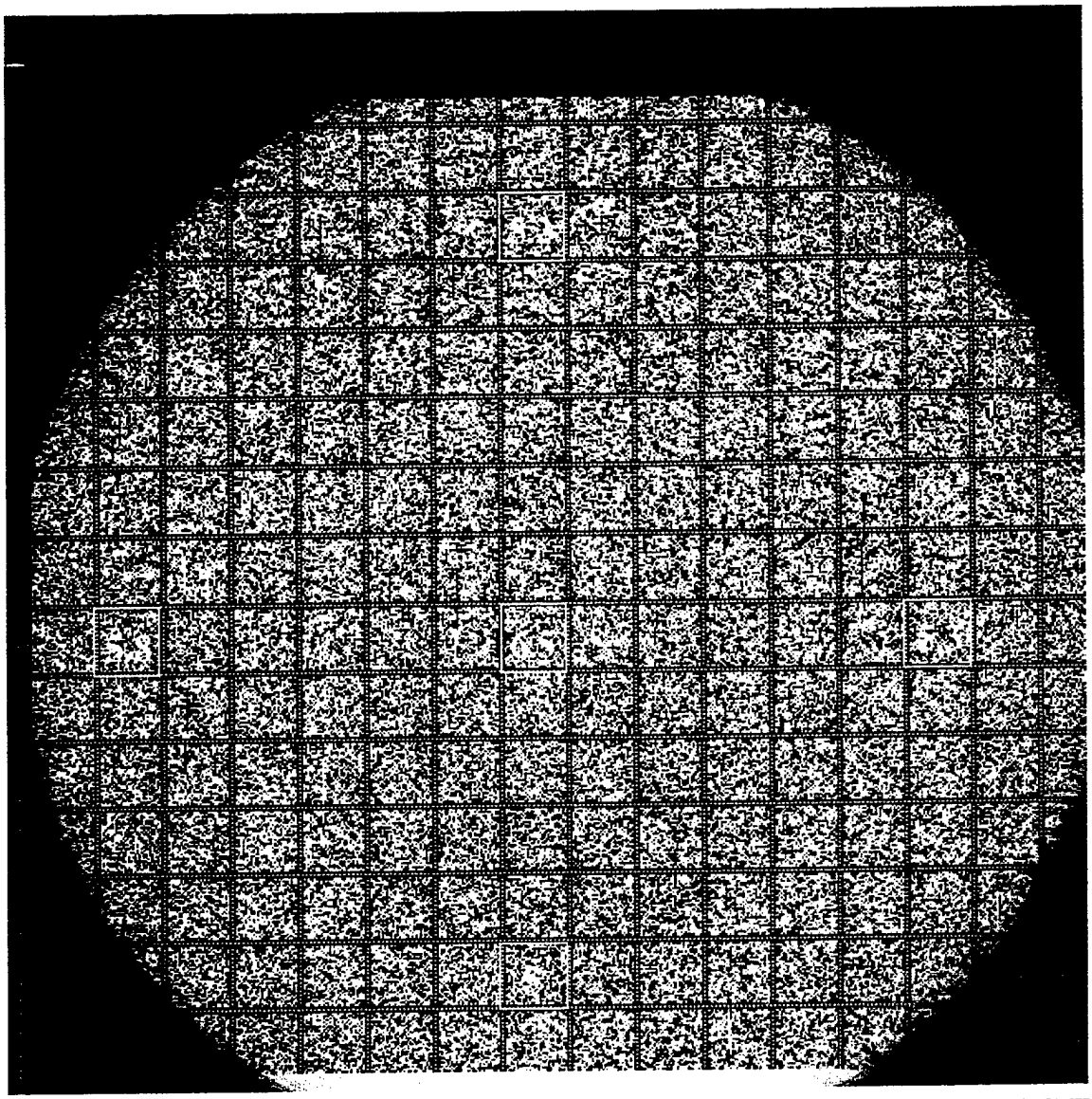

Figure 4.2: A data pattern imaged from the SLM to the CCD array with computed SNR in different regions.

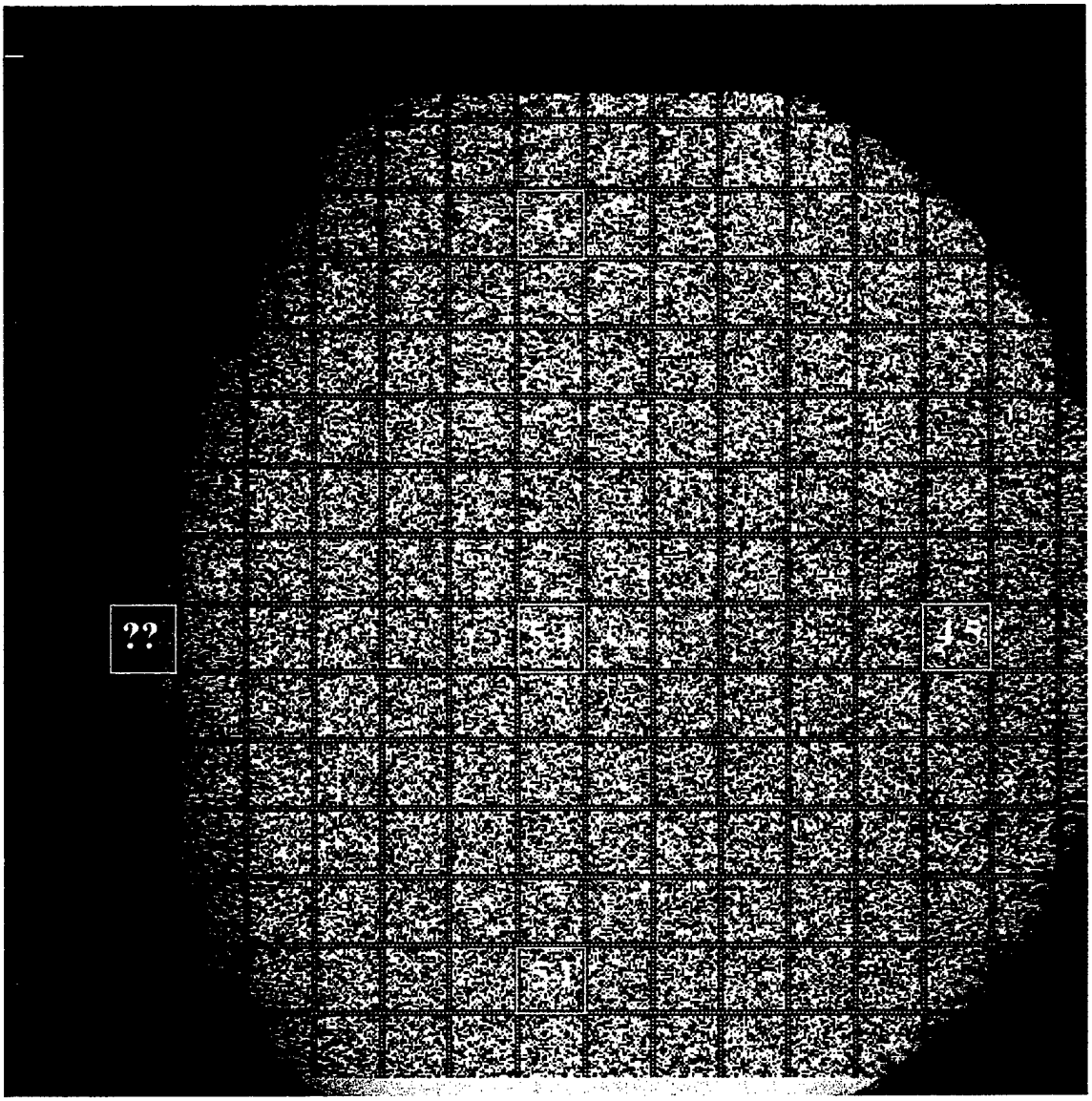

Figure 4.3: A reconstruction from a single hologram recorded in DuPont's photopolymer using the high density setup.

In designing the high density recorder setup, we chose to have the signal beam on-axis and the reference off-axis by 60° to maximize the total number of pixels that can be read out simultaneously with the reference beam de-tuned to the optimum angle (anticipating a 3% shrinkage). For the one hologram experiment (Figure 4.3), more than 120,000 out of 180,000 pixels (67%) is pixel-to-pixel match and has sufficient intensity to be read. The other 60,000 pixels can be read by de-tuning the reference beam angle slightly off of the optimum angle (to Bragg match the left region instead of the middle). This means we might have to read the same hologram several times with slightly difference reference beam angles to get the complete data frame. There are other methods to compensate for the shrinkage effect and we will discuss them later in this section.

With a single hologram stored, the surface density is only 0.5 bit/μm^2. However, by multiplexing a number of holograms at the same spot, we can increase the surface density

dramatically. From the one hologram experiment we noticed that if the recording material was rotated by 60° peristrophically during reconstruction, the recalled hologram becomes invisible to the CCD array (due to Bragg mis-match and change in deflection angle). This means up to 6 different peristrophic holograms can be stored at the same location by rotating the recording material the full 360°. Furthermore, we can also multiplex a number of angle holograms at each peristrophic position to increase the density even more. In one experiment, we multiplexed a total of 21 holograms at a single location by recording 7 angle holograms at each of the 3 peristrophic positions. The angle holograms were separated by 2.5° and the peristrophic positions were separated by 60°. At .5 bit/μm^2 per hologram, this gives an effective surface density of 10.5 bits/μm^2. For comparison, a surface density of 10.5 bits/μm^2 is approximately twice the density of a single layered DVD. Figure 4.4 shows a reconstructed data pattern from one of the 21 holograms stored. This particular frame was the 17th hologram stored (the 3rd angle hologram in the last peristrophic position. The SNR measured in the 21 holograms experiment are significantly lower than that of the 1 hologram experiment. This is mostly due to the additional cross-talk noise introduced between the different angle multiplexed holograms. An interesting note to point out is where as in the 1 hologram experiment the SNR at the left side of the data frame could not be computed due to shrinkage, it now can be computed for Figure 4.4. This is because the shrinkage effect is a real-time process. The DuPont photopolymer material shrinks continuously with exposure to light until the entire dynamic range is exhausted. Therefore, holograms recorded earlier suffer more shrinkage than later holograms. For example, the intensity profile of the reconstruction from the 1st recorded hologram in the 21 holograms experiment looked similar to the 1 hologram experiment. By the 17th hologram (for the 21 hologram experiment), the shrinkage effect was weak enough to allow the entire data frame to be pixel-matched and read out simultaneously.

Continuing on with our quest for higher density, we doubled the number holograms stored by recording 7 angle holograms at each of the 6 peristrophic positions (for a total of 42 holograms stored). Each peristrophic position is separated by 60° and the full 360° rotation is utilized. The angle holograms are still separated by 2.5°. At .5 bits/μm^2 per hologram, this gives an effective surface density of approximately 21 bits/μm^2. Figure 4.5 shows the reconstruction from the 38th hologram of the 42 holograms experiment. The SNR in Figure 4.5 does not differ significantly from Figure 4.4 (the 21 holograms experiment). This is because (1) additional peristrophic holograms do not introduce significant cross-talk noise when the separation is sufficient (determined previously to be 60°); (2) the DuPont photopolymer has sufficient dynamic range to support 42 holograms without degradation. Unlike angle multiplexing, the deflection direction of the peristrophic hologram changes as the recording material is rotated. The 60° in peristrophic rotation changes the deflection angle enough so that the CCD array no longer sees the reconstructed data frame. Therefore, there is no cross-talk between peristrophic holograms.

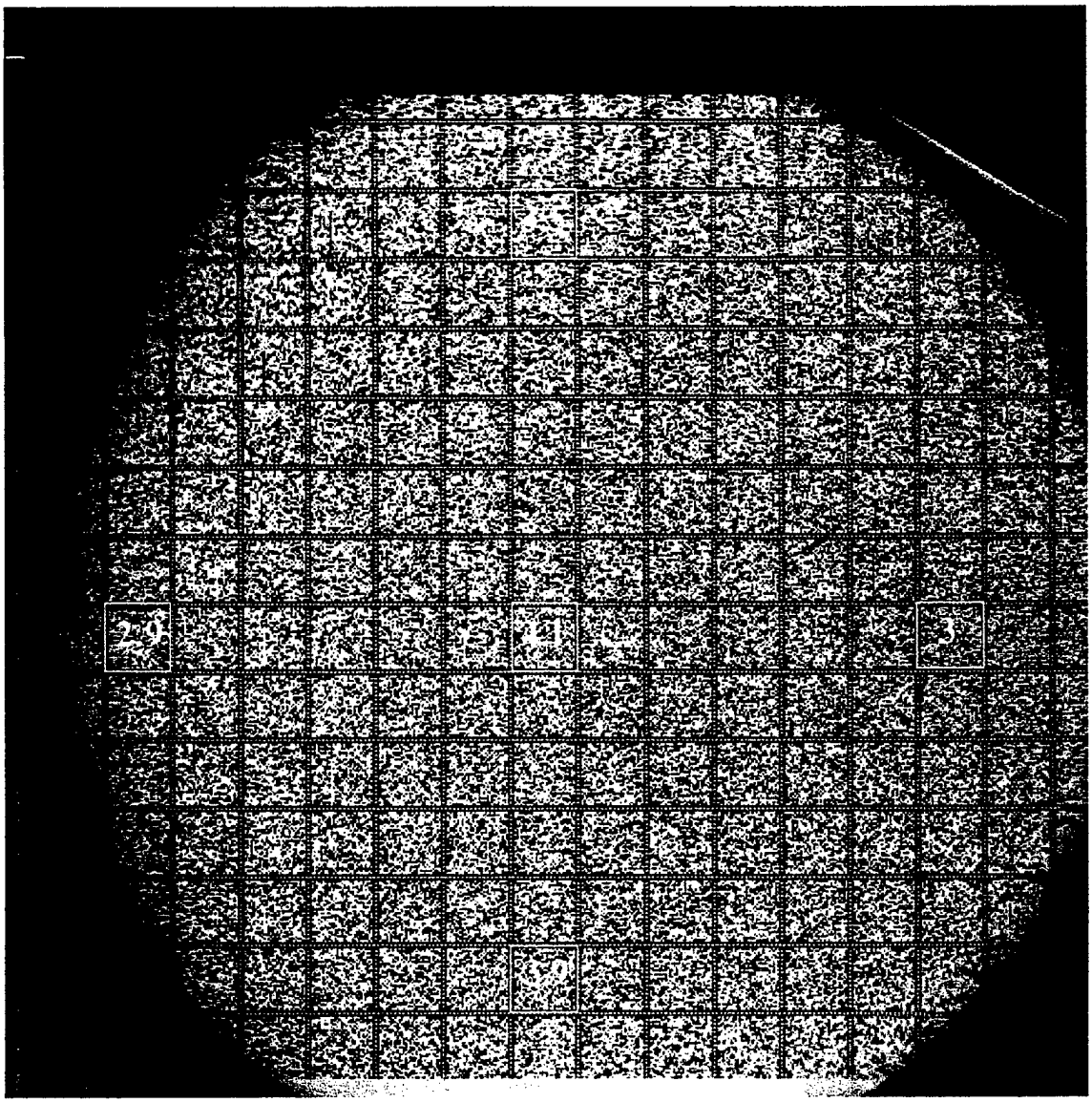

Figure 4.4: Reconstruction of the 17th hologram from the 21 holograms experiment.

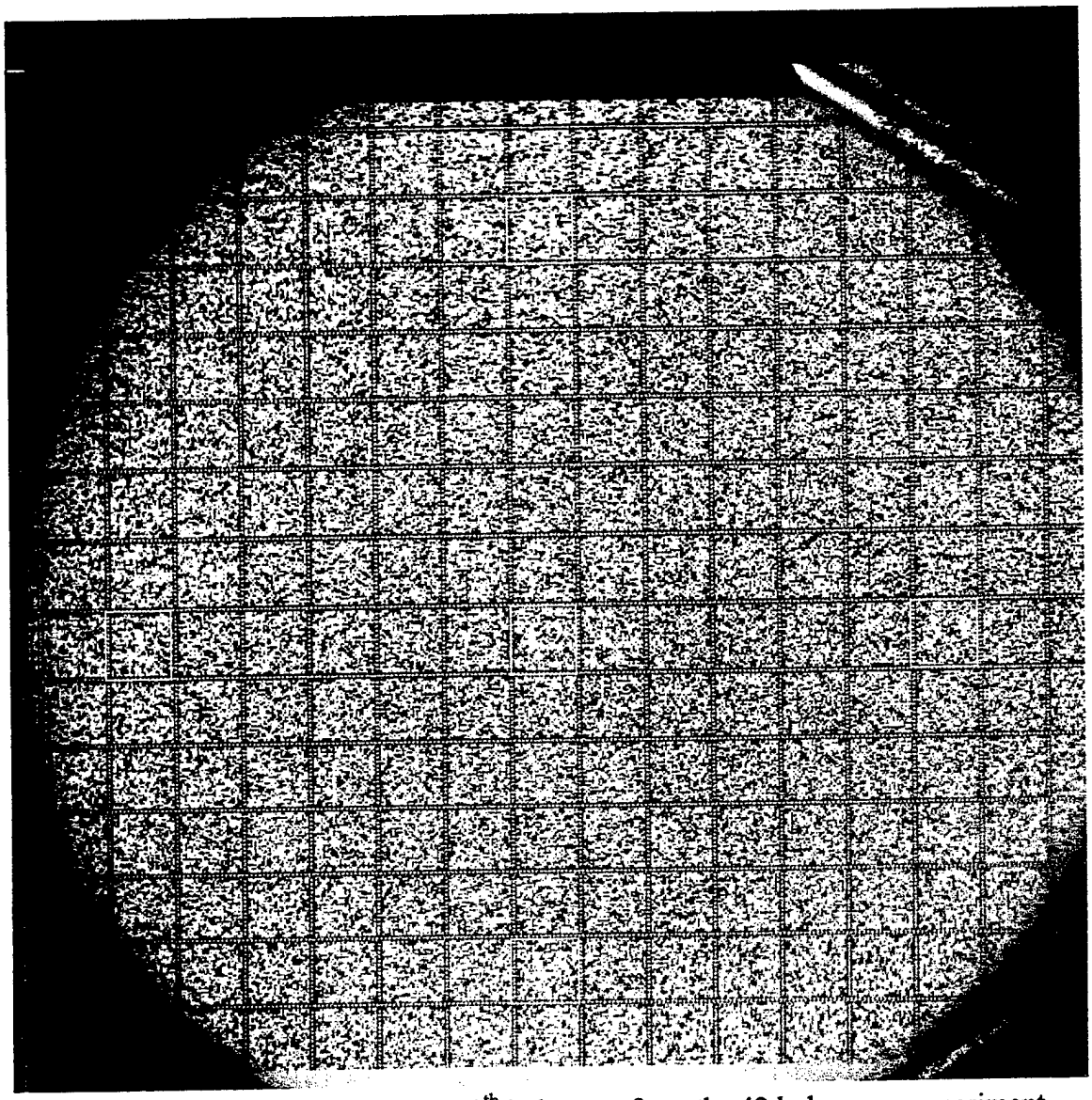

Figure 4.5: Reconstruction of the 38th hologram from the 42 holograms experiment.

To further increase the surface density (by increasing the number of holograms stored at a single location) it is now necessary to decrease the separation between the angle holograms since all the possible peristrophic positions are used. To achieve a surface density of 30 bits/μm^2, 60 holograms will have to be multiplexed at the same location. With 6 peristrophic positions, that means 10 angle holograms at each peristrophic position. Separating the angle holograms by 2° (instead of 2.5° as in the 21 bits/μm^2 experiment), we will still be within the scanning range of the setup. Figure 4.6 shows the reconstruction from the 55th stored hologram of the 60 holograms experiment. The average SNR of this experiment is slightly lower than the 21 bits/μm^2 experiment shown previously. This is mostly due to the additional cross-talk noise introduced when the angular separation was reduced. Furthermore, the dynamic range of the recording material is beginning to show signs of exhaustion, resulting in weaker holograms overall. For a hologram to have good SNR, its diffraction efficiency must be significantly above the scattering diffraction efficiency of the recording material. The scattering diffraction

efficiency is defined as the power scattered by the recording material (within a defined solid angle such as the aperture of the f/1.1 lens) divided by the incident power. The scattering diffraction efficiency for a given material and setup is fixed and each stored hologram must have sufficient diffraction efficiency to overcome the scattering diffraction efficiency for good SNR. For our experiments, nearly the entire dynamic range of the recording material is divided equally among the holograms stored. Therefore, the more holograms we store, the less each hologram gets (and smaller the diffraction efficiency).

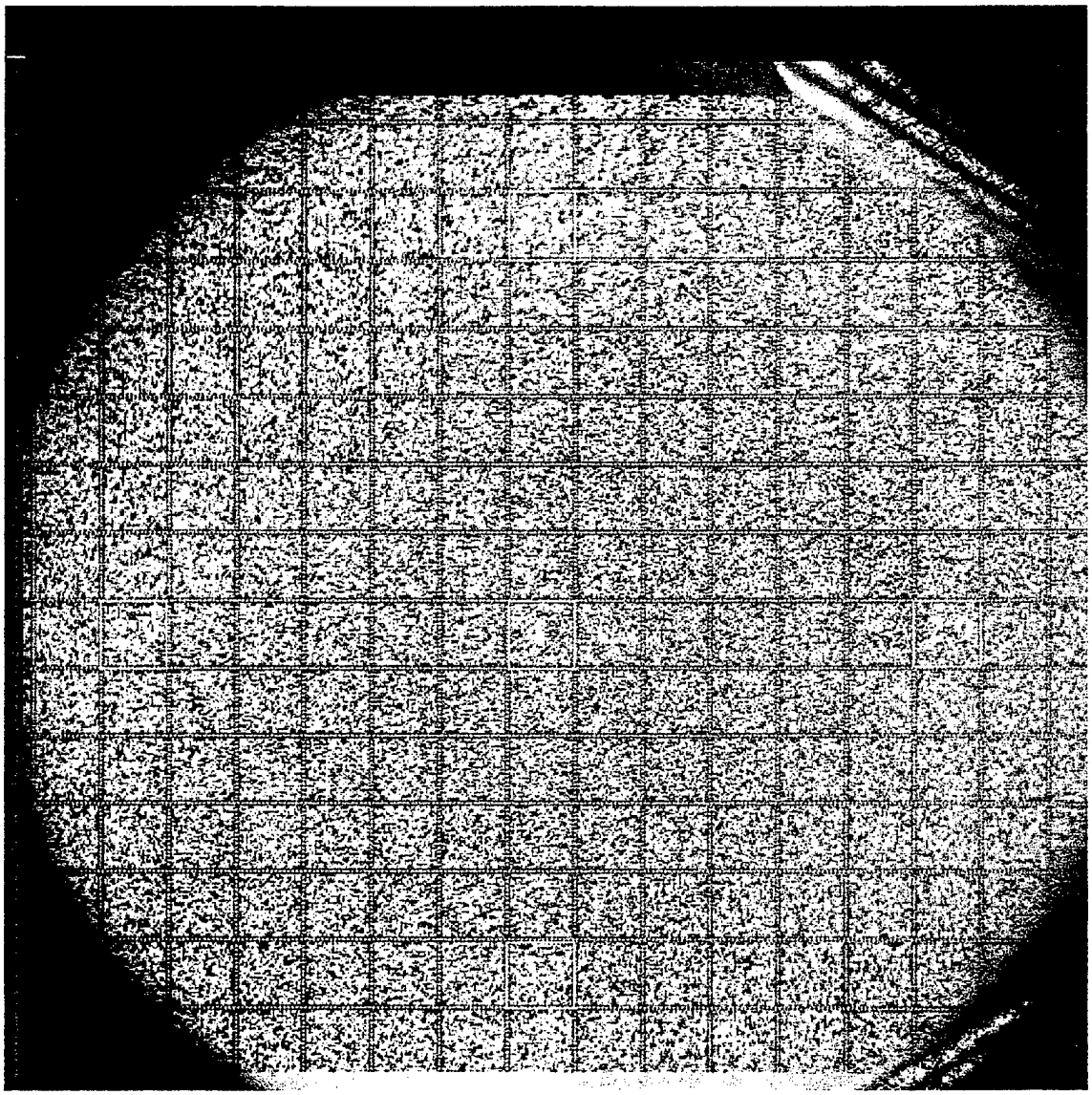

Figure 4.6: Reconstruction of the 55th hologram from the 60 holograms experiment.

To achieve our surface density goal of 40 bits/μm^2, it is necessary to decrease the angular separation even further from 2° to 1.8° so more holograms can be multiplexed at a single location. Each of the 6 peristrophic positions was separated by 60° and 14 angle holograms were stored at each peristrophic position. This gives a total of 84 holograms stored at a single location with a storage density of 42 bits/μm^2. Figure 4.7 shows the reconstruction from the 77th stored

hologram of the 84 holograms experiment. The average SNR of the 42 bits/μm^2 experiment is actually better than the 30 bits/μm^2 experiment shown previously. This is most likely due to the extra care we took to reduce noises in the setup and better alignment. Furthermore, an angular separation of 1.8° is closer to the Bragg null than 2°, therefore less angular cross-talk is experienced. Table 4.1 shows an overview of all the high density experiment.

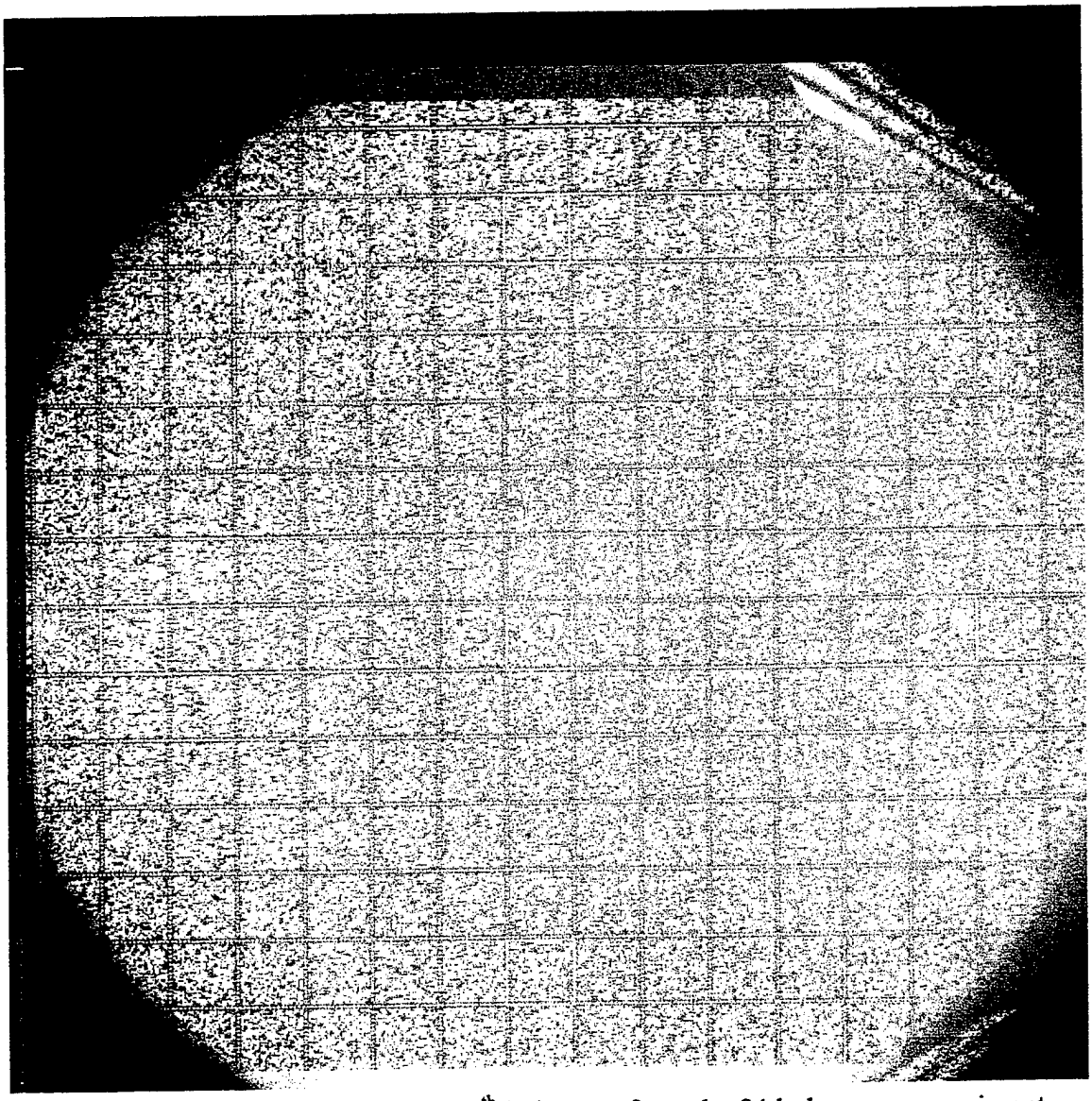

Figure 4.7: Reconstruction of the 77th hologram from the 84 holograms experiment.

	Density	Average SNR	Angle Holograms	Angular Separation	Peristrophic Holograms	Peristrophic Separation
SLM to CCD	NA	5.6	0	NA	0	NA
1 Hologram	0.5 bit/μm^2	5.0*	1	NA	1	NA
21 Holograms	10.5 bits/μm^2	3.5	7	2.5°	3	60°
42 Holograms	21 bits/μm^2	3.4	7	2.5°	6	60°
60 Holograms	30 bits/μm^2	3	10	2°	6	60°
84 Holograms	42 bits/μm^2	3.4	14	1.8°	6	60°

Table 4.1: An overview of the high density experiments (*averaged without the left region).

In the above discussions we have shown the experimental setup and results from no hologram stored all the way up to 42 bits/μm^2. From this data, we would like to identify all the significant noise sources so that the SNR and the BER of the holograms can be improved. The first source of noise that comes to mind is the CCD and digitizer noise. The Philips FTT1010 CCD and digitizer we used were designed to have very low electronic noise. We measured their impact on the SNR of the recalled holograms for this setup by flooding the detector array with a controlled and uniform light source and then measuring the variance of the digitized output for different illumination intensity. Figure 4.8 shows the result. From Figure 4.8 we can compute the degradation in SNR caused by the CCD and digitizer. Previously a random data frame from the Kopin SLM was imaged with the custom designed lenses through a 1 mm thick glass onto the CCD array (Figure 4.2). The resulting mean value for the dark (zero) pixels is μ_d=55 and the variance of the dark pixels is σ_d^2=103 (for the middle region). Similarly, the mean and the variance for the bright (one) pixels are μ_b=203 and σ_b^2=412, respectively (for the middle region). Using our method of computing the SNR (Equation 2.2), the resulting SNR=6.53. This SNR includes noises from the laser, SLM, imaging lenses, and the CCD+digitizer so we will call it $SNR_{laser+SLM+imaging+CCD}$=6.53. If we subtract out the variances coming from the CCD+digitizer using Figure 4.8 and then re-compute the SNR, we get $SNR_{laser+SLM+imaging}$=6.59. What this means is that a gain of 0.05 in SNR is possible if we had a CCD+digitizer combination that was noiseless. Since this gain is so small, we will just assume that the Philips FTT1010 CCD and digitizer are ideal.

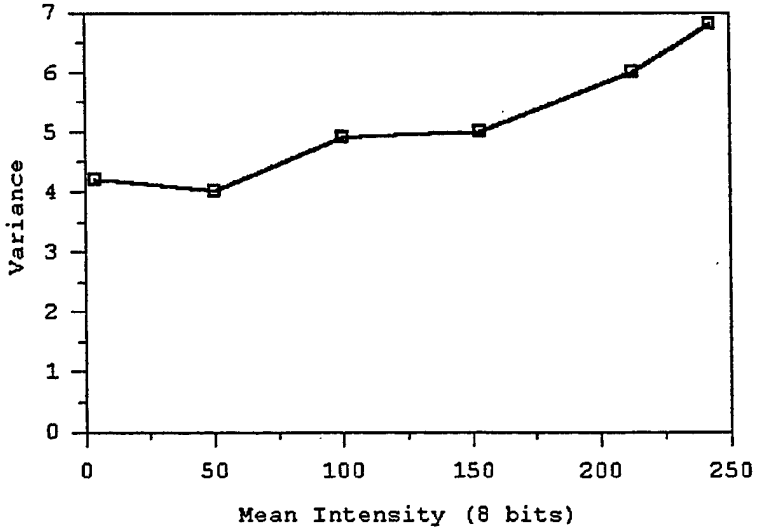

Figure 4.8: Variance of the Philips FTT1010 CCD/digitizer as a function of incident intensity.

Another source of noise is the custom designed imaging lenses that images the SLM onto the CCD. From theoretical calculations using the point-spread-function (PSF) of the lenses (obtained from a ray-tracing program using the specifications of the lens) and ideal 24 μm pixel pitch SLM+CCD, we get μ_d=8, σ_d^2=26, μ_b=216 and σ_b^2=152, for a random bit pattern imaged. Using Equation 2.2 it can be computed that the best SNR possible using our custom designed lenses (assuming everything else is perfect) is $SNR_{imaging}$=15.6. This indicates that the lenses in the setup can achieve a BER much better than 10^{-6} if the laser, SLM, and recording material are ideal.

We can also re-normalize the means and variances for $SNR_{imaging}$ and then subtract the resulting variances from $SNR_{laser+SLM+imaging}$ to get $SNR_{laser+SLM}$=7.6. $SNR_{laser+SLM}$ is the best SNR possible using the current laser and Kopin SLM if everything else is ideal. The big drop in SNR from $SNR_{imaging}$ to $SNR_{laser+SLM+imaging}$ indicates that the laser and/or Kopin SLM is very noisy. We believe the Kopin SLM is the major contributor of noise because when the same SNR measurement was conducted using a chrome mask instead of the Kopin SLM, the resulting SNR was much better (Section 2). When a single hologram was recorded, we measured its $SNR_{laser+SLM+imaging+media+1\ hologram}$ to be 5.4 (middle region). By subtracting out $SNR_{laser+SLM+imaging}$, we get $SNR_{media+1\ hologram}$ = 8.7. This shows that the best SNR possible with the DuPont photopolymer and the process of recording one hologram in it is 8.7, assuming all else ideal. When compared with $SNR_{laser+SLM}$, it shows that the SNR of a single hologram is more limited by the Kopin SLM than the recording material/recording process. For multiplexed holograms, $SNR_{media+21\ holograms}$ = 5.4, $SNR_{media42\ holograms}$ = 5.5, $SNR_{media+60\ holograms}$ = 5.1, and $SNR_{media+84\ holograms}$ = 4.9.

The drop in SNR from 1 to many holograms is most likely due to cross-talk noise between the angle holograms. For the 21 and 42 holograms experiments, the separation between the angle holograms were the same at 2.5° while for the 60 holograms experiment, the separation was 2°. Therefore, $SNR_{media+60\ holograms}$ is noticeably lower than $SNR_{media+21\ holograms}$ and $SNR_{media+42\ holograms}$. The small drop in $SNR_{media+84\ holograms}$ when compared with $SNR_{media+60\ holograms}$ is mostly due to the lower diffraction efficiency per hologram from storing more holograms. Table 4.2 shows a list of SNR for this series of experiments.

The associated bit-error-rate (BER) for $SNR_{media+84\ holograms}$ = 4.9 is in the 10^{-4} to 10^{-5} range. With error-correction-codes (ECC), it would be a simple matter to bring the BER to 10^{-12} for the 42 bits/μm^2 experiment. The real challenge so far is with the recording material shrinkage effect. As shown previously, the undesirable effects of photopolymer shrinkage include : (1) the reference beam has to be de-tuned to maximize diffraction efficiency during readout (due to a change in the grating frequency); (2) the total number of pixels per hologram available for parallel readout is reduced (due to the inability to Bragg match the entire hologram with a single planewave reference beam); (3) The SNR of the reconstructed hologram is reduced non-uniformly across the data frame (due to a slight spatial distortion in the reconstruction).

Method	SNR	Value	Note
Theoretical	$SNR_{imaging}$	15.6	Best SNR possible with custom lenses
Experimental	$SNR_{laser+SLM+imaging}$	6.5	SNR measured using all the components of the high density setup
Computed	$SNR_{laser+SLM}$	7.6	Best SNR possible with the laser and Kopin SLM
Computed	$SNR_{media+1\ holograms}$	8.7	Best SNR possible from a single hologram recorded in DuPont photopolymer
Computed	$SNR_{media+21\ holograms}$	5.4	Best SNR possible from 21 holograms recorded in DuPont photopolymer
Computed	$SNR_{media+41\ holograms}$	5.4	Best SNR possible from 42 holograms recorded in DuPont photopolymer
Computed	$SNR_{media+60\ holograms}$	5.1	Best SNR possible from 60 holograms recorded in DuPont photopolymer
Computed	$SNR_{media+84\ holograms}$	4.9	Best SNR possible from 84 holograms recorded in DuPont photopolymer

Table 4.2 : A list of SNR for the high density experiments (for the middle region of the date frames).

We can deal with these problems in the design of our system using three different approaches. (1) De-tune the reference beam until maximum diffraction efficiency and then readout a subset of the reconstructed data frame where the SNR is sufficient. (2) Correct the shrinkage problem during the recording process by using a special reference beam that is shrinkage insensitive. (3) Use a recording material that has lower shrinkage than DuPont's photopolymer. Method (1) reduces both the storage density and the transfer rate of the system because fewer pixels than the system can support is stored and read. Method (2) restricts the recorder and reader to a particular geometry using a special reference beam. This special reference beam might make the system more sensitive to alignment errors. Method (3) seems to be the most straightforward solution to the shrinkage problem. One material that shows promise from initial publications is a photopolymer formulation from Polaroid. This material has a "ring-opening" structure, meaning in order for the monomer to polymerize, the monomer has to break a bond which increases its volume initially. Monomers with "opened-rings" then polymerize and its size becomes more compact. Since monomers were slightly expanded initially, the final volume change is small. In terms of volume change, we have measured the DuPont HRF-150 material to have a shrinkage of ~3%. Polaroid claims a volume shrinkage of less than 1% for their photopolymer.

We have received many photopolymer samples from Polaroid and provided much feedback in the direction in which this material should be improved. The recording characteristics of one batch from Polaroid is shown in Figure 4.9. The active part of the material is about 100 microns thick and is sandwiched between two pieces of 1.5 mm thick glass slides (it is in liquid form until polymerized). The Polaroid material requires around 15 mJ/cm^2 of exposure energy to become sensitized and then exhibits a quasi-linear recording behavior (the grating strength grows linearly with respect to the exposure energy) until around 70 mJ/cm^2. At that point, the material is nearly depleted of monomers so the grating strength begins to saturate and the curve levels off. The 'knee' of the curve indicates that saturation is at around 110

mJ/cm^2. The final cumulative grating strength of Figure 4.9 shows the M/# of the material to be around ~3.2 (when a fix number of holograms are multiplexed, the higher the M/#, the higher the diffraction efficiency per hologram).

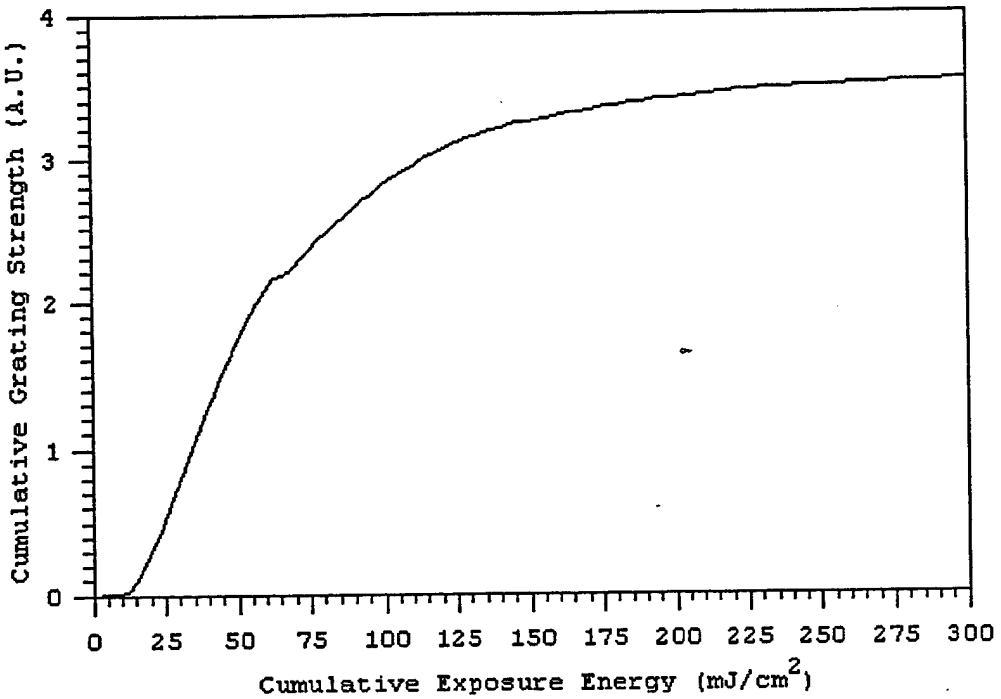

Figure 4.9: Recording characteristics of Polaroid's photopolymer from one particular batch.

For comparison, the DuPont HRF-150 photopolymer requires 35 mJ/cm^2 to sensitize, 150 mJ/cm^2 to saturate (at the 'knee'), and the final cumulative grating strength is around 6.5. So the DuPont material is slightly less sensitive when compared to the Polaroid material but it achieves a much higher final cumulative grating strength. Figure 4.10 shows a data frame imaged through a cured sample of the Polaroid material. The SNR of the resulting data frame is lower than the same data page imaged through DuPont's photopolymer (Figure 4.2). This reduction in SNR is mostly due to the thickness of the samples Polaroid provided. The Polaroid photopolymer in its original state is a liquid, therefore it must be sandwiched between two pieces of glass. The glass plates Polaroid used are of high optical quality but thick (1.5 mm per slide). Therefore, the Polaroid samples are about 3.1 mm thick instead of the DuPont samples we regularly prepare at 1.1 mm thick. When we designed our imaging lenses for the high density recorder, we factored in a recording material thickness of around 1 mm. The thicker Polaroid material causes additional spherical aberration which when combined with lens imperfections reduced the SNR of the imaged data frame. Furthermore, the thicker samples also made the setup more sensitive to misalignments and tilts (the two glass plates might not be completely parallel). To correct the thickness problem, we have shipped thinner glass substrates to Polaroid (0.8 ~ 1 mm thick).

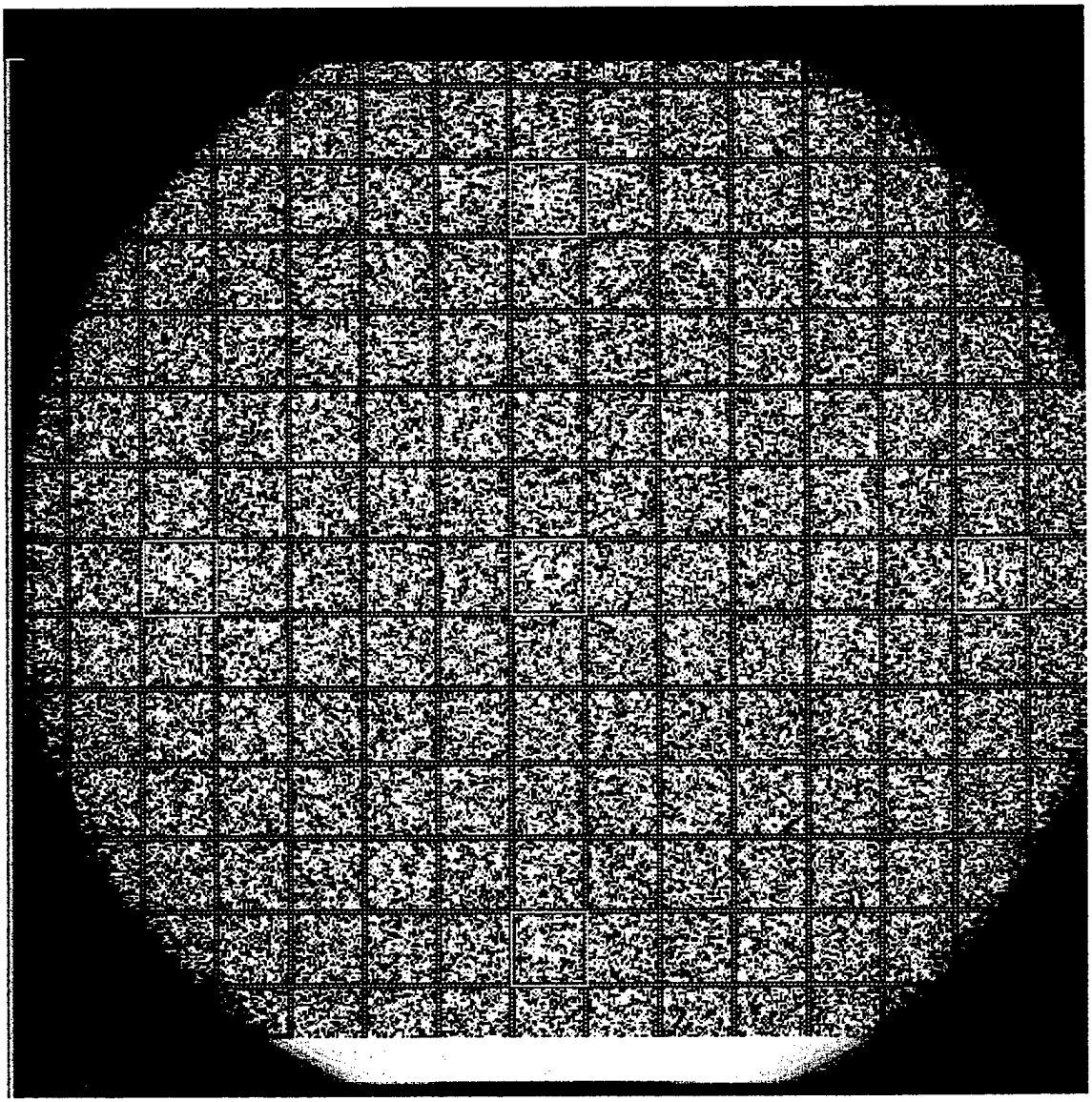

Figure 4.10: A data frame imaged from the SLM through a cured sampled of the Polaroid photopolymer to the CCD array.

Figure 4.11 shows the reconstruction of a single hologram recorded in the Polaroid material. Notice the SNR dropped very little when compared to Figure 4.10. This means the Polaroid material can record high density holograms with good fidelity. Furthermore, the entire hologram can be readout in parallel (after de-tuning the reference beam to maximize diffraction efficiency). As shown in Figure 4.3, a single hologram recorded in DuPont's material cannot be reconstructed in its entirety due to higher shrinkage.

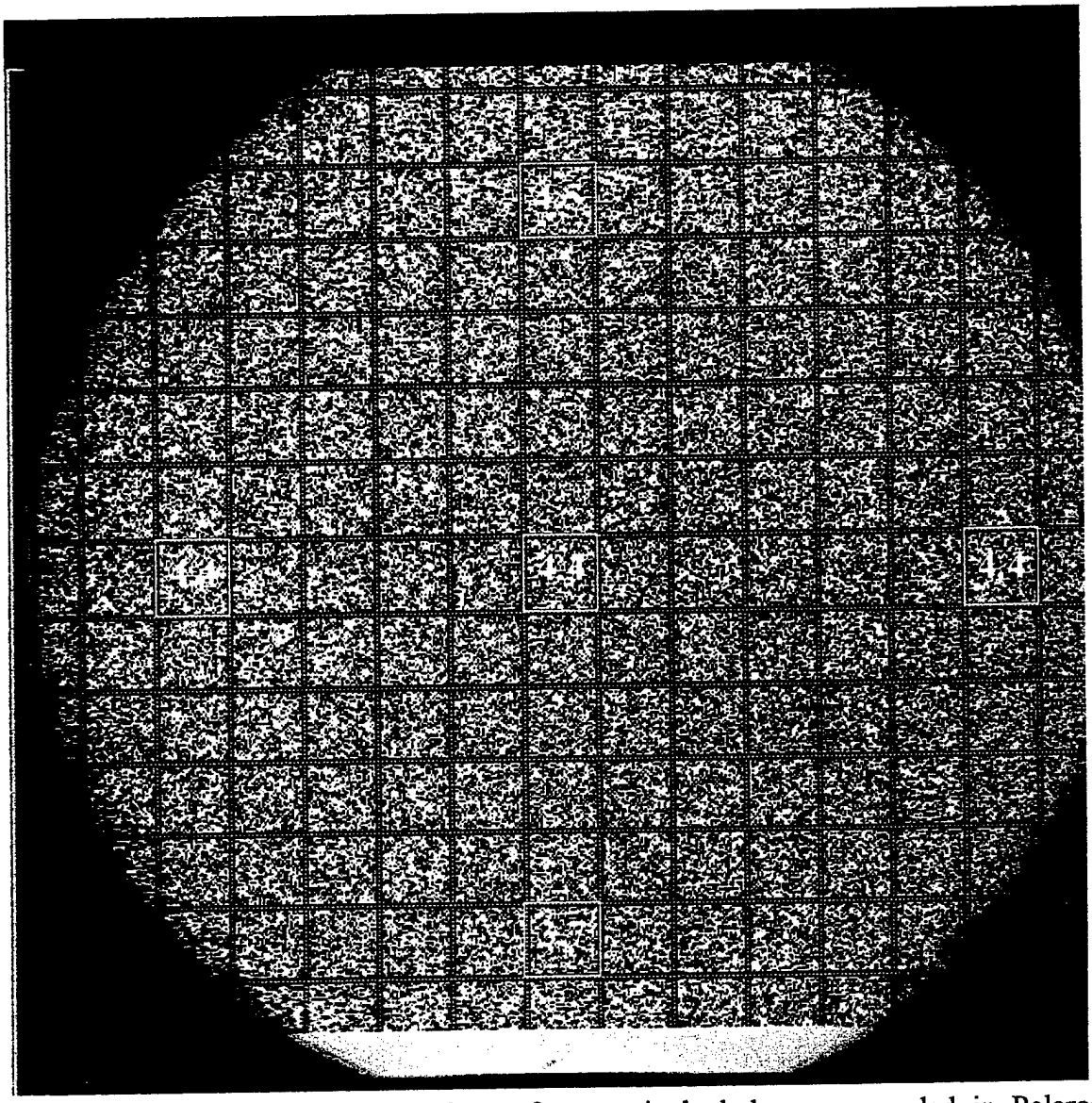

Figure 4.11: The reconstructed data frame from a single hologram recorded in Polaroid's photopolymer.

Another advantage of the Polaroid material is that it is sandwiched between two pieces of high quality glass. Therefore, its surface quality is very good. Using the same interferometer setup shown in Figure 2.3, we tested the Polaroid samples. Figure 4.12 shows the interference pattern generated with a Polaroid photopolymer sample in one of the arms of the interferometer. The lines remained straight and parallel indicating good optical quality. The period varied slightly from left to right probably due to the two cover glass plates not completely parallel with one another. With good optical quality, good sensitivity, little shrinkage, and good dynamic range, the Polaroid material shows significant promise and we hope to test it further by multiplexing many holograms at a single location when sufficient quantity of this material becomes available.

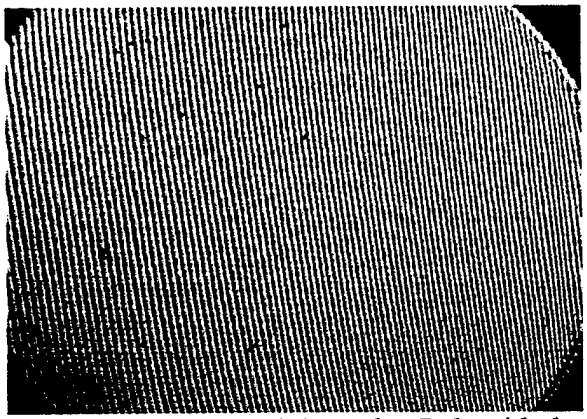

Figure 4.12: Interference pattern imaged through a Polaroid photopolymer sample.

Previously we also briefly mentioned using a special reference beam to correct the material shrinkage problem during recording. This method of fixing the shrinkage problem could be useful if a better recording material cannot be found (or does not 'materialize'). The theoretical background for this "shrinkage-insensitive" recording geometry is as follows. For the high density holograms recorded with a planewave reference beam (as in our setup), portions of the recorded gratings would lift-off or dive below the κ-sphere due to shrinkage. These Bragg-mismatched portions can be brought back on the κ-sphere by changing the reference beam angle slightly during reconstruction. However, the deflection angle of the re-Bragg matched portion is slightly different when compared to the original signal direction and only a portion of the entire hologram can be Bragg matched at a time. It might be possible to use a cylindrical reference beam to re-Bragg match the entire hologram at the same time. However, the reconstructed data frame would still be a little bit compressed.

Instead of trying to re-Bragg match the shrunken gratings during reconstruction, is there a way to prevent the gratings from shrinking in the first place? Specifically, can we use the ray nature of a spherical reference beam to record shrinkage insensitive hologram? It is known for gratings recorded with symmetric rays (with respect to the recording material's surface normal), shrinkage has no effect on its Bragg condition. Figure 4.13 (a) shows a planewave reference beam interfering with a high bandwidth signal beam to produce a high density hologram (neglecting Snell's law). The angle of the reference beam is symmetric with the center ray of the signal beam. Therefore, that portion of the hologram will remain Bragg matched after shrinkage. This is shown in the k-sphere diagram of Figure 4.13 (b).

However, the planewave reference beam has only one incident angle so it cannot record symmetric holograms with all the rays in the signal beam. This is where the spherical reference beam comes in. Figure 4.14 (a) shows a spherical reference beam recording a hologram with a high bandwidth signal beam. The focal point of the signal beam is in front of the recording material and the focal point of the spherical reference beam is behind. The lenses that produce the cone of rays for the signal and reference arms have the same $f/\#$. When the rays are positioned properly as shown, the entire hologram is formed by symmetric rays. More specifically, a pair of symmetric signal and reference rays form a single grating at a localized area. This is repeated through out the entire hologram. Since the gratings have no z-components, photopolymer shrinkage has no effect on their Bragg conditions. This is shown in the κ-sphere diagram of Figure 4.14 (b) for three grating vectors.

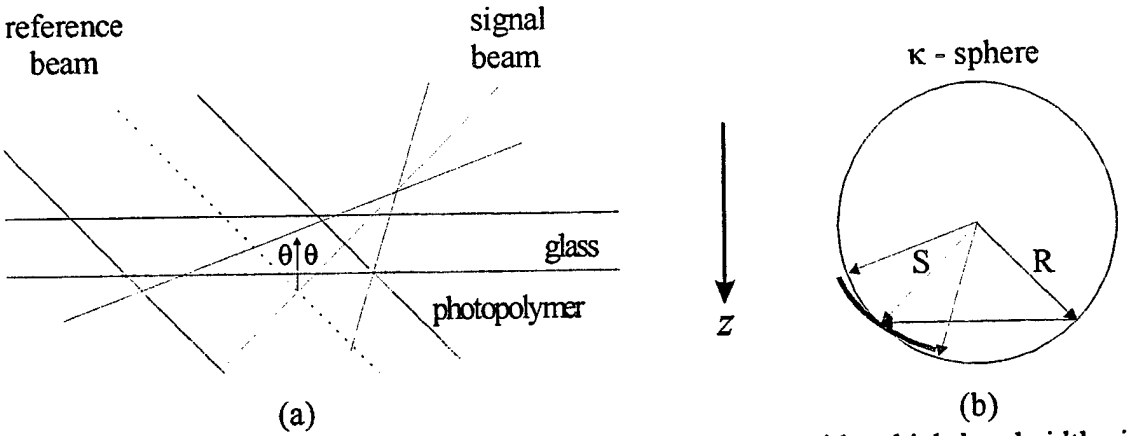

Figure 4.13: A planewave reference beam recording a hologram with a high bandwidth signal beam. (a) The recording geometry. (b) The κ-sphere diagram after shrinkage.

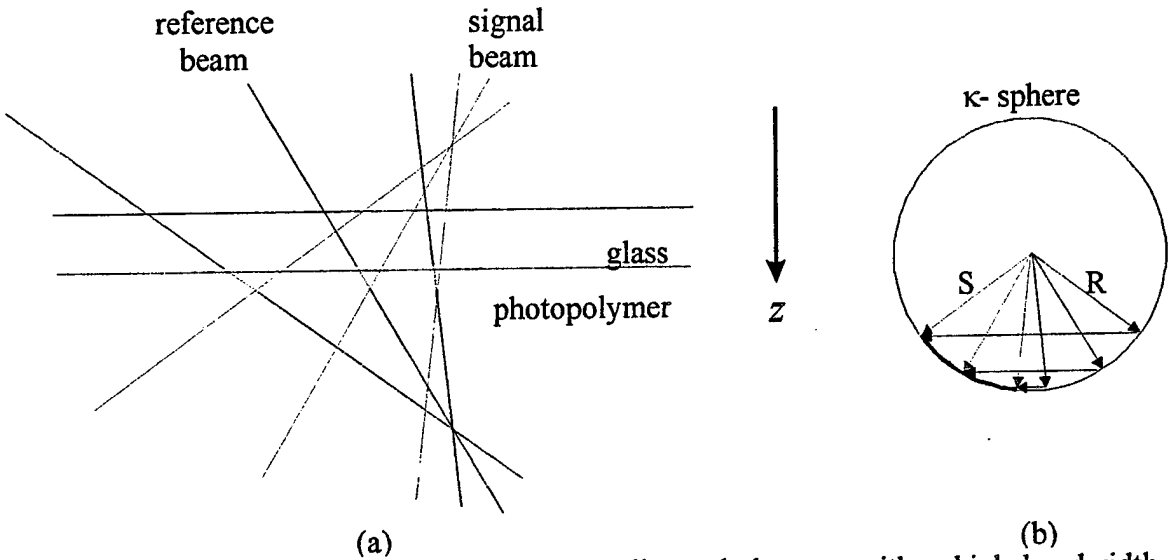

Figure 4.14: A spherical reference beam recording a hologram with a high bandwidth signal beam in the shrinkage insensitive geometry. (a) The rays of the signal and reference beams in the setup. (b) The κ-sphere diagram after shrinkage.

To demonstrate that this shrinkage insensitive geometry actually works, we used basically the same high density setup as shown in Figure 4.1. Figure 4.15 shows the shrinkage insensitive recording geometry setup. Instead of using a planewave to record the hologram, a spherical reference beam is generated by a *f*/1.1 CCD camera lens. The rays are positioned so that the signal beam spot on the photopolymer is covered by the reference beam spot and the center ray of the signal and reference beams overlap symmetrically with respect to the photopolymer's surface normal (at $\pm$ 35°).

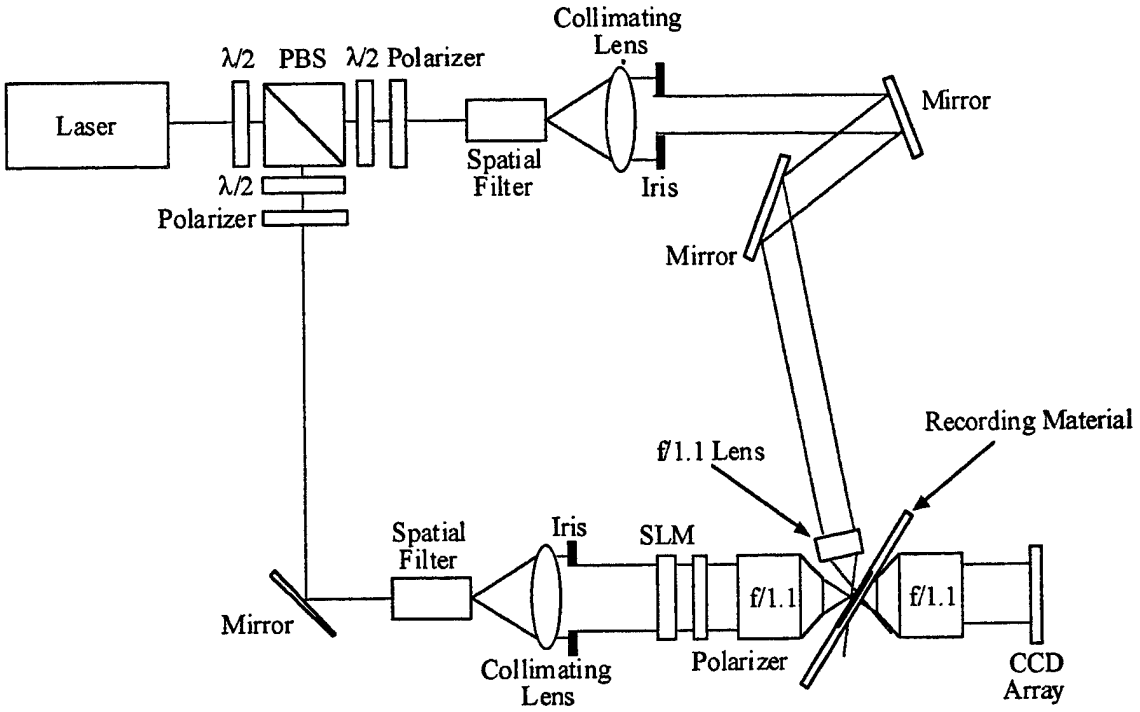

Figure 4.15: The high density shrinkage insensitive setup using a spherical reference beam.

Figure 4.16 shows the resulting reconstruction for a hologram recorded with a spherical reference beam in the shrinkage insensitive geometry. The entire reconstruction is visible at the same time so there is no need for any re-Bragg matching. Furthermore, the reconstructed image is not distorted or compressed in any direction since the gratings did not suffer any shrinkage effect. This shows that the shrinkage insensitive geometry works. One side effect of using a spherical reference beam is the non-uniform intensity in the reconstructed hologram. This is caused by the gaussian intensity profile of the focused reference beam and can be corrected by using a spatially varying attenuator. An interesting advantage of using a spherical reference beam to record holograms is its direct connection to a simple multiplexing method called 'shift multiplexing'. Shift multiplexing is especially well suited to the holographic 3-D disk application because it is very similar in design to the current compact disc. However it is beyond the scope of this project to experiment with shift multiplexing extensively so we will keep the spherical reference beam as a possible method to correct for material shrinkage.

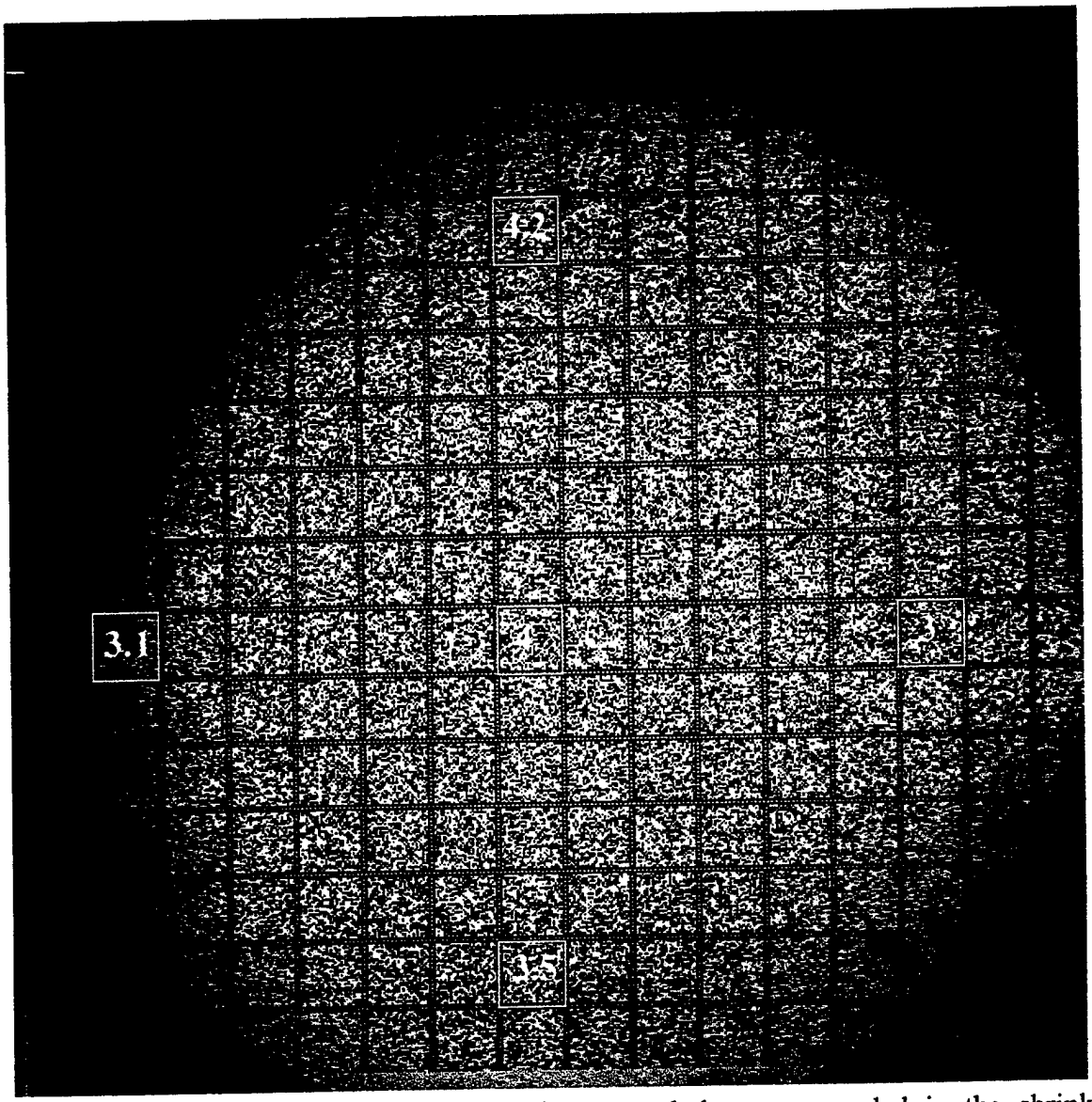

Figure 4.16: The reconstructed data frame from one hologram recorded in the shrinkage insensitive geometry.

5.0 System Level Demonstration

Following the parameters of the proposal, the current system uses a 12 cm diameter disk, SLM size of 480 pixels in diameter, and a recording area per location of 0.33 mm^2. We were able to extend the scanning range of the reference beam to 23° and stored a total of 84 holograms at a single location (as compared to 20° and 80 holograms with the proposed system). This gives us 42 bits/μm^2 and a disk capacity of 0.35 Tbits per side. The random access time of the disk matches the proposed 17ms when spinning at 3600 RPM.

For recording rate and readout rate, the performance of the current system is limited by the electronics in the setup. For the current system, a reconstructed data frame containing 180,000 pixels (bits) is readout at a frame rate of 30 Hz using the Philips CCD array. This gives a readout rate of 5.1 Mbits/s, far short of the proposed 1 Gbits/s. To reach 1 Gbits/s, we need to have a data frame with 1,000,000 pixels readout at 1 KHz. This means we need to have a SLM with 1150 pixels in diameter and a CCD array capable of 1 KHz operation, both of which are hard to come by at this time (the TI DMD chip can switch at the KHz level but would need custom electronics). The recording rate for the current system is at 240 Kbits/s. This is achieved by recording a hologram (with 180,000 pixles) in .7 seconds on the average. The reason why it takes so long to record a hologram is because the computer controlled rotational stage is slow. It takes about half of a second to move 1° (in high accuracy mode). Another problem is with the low efficiency (throughput) of the Kopin SLM (less than 10%). This means the amount of laser power falling on the recording material during recording is low, therefore it takes longer to record a hologram. To demonstrate that high speed recording can be achieve if the SLM and rotational stage were not a problem, we replaced the computer controlled rotation stage with a galvo scanner and removed the SLM from the setup. We were then able to record 200 holograms in 200 ms (1 ms per hologram). If each hologram had contained 180,000 pixels, this translates to a recording rate of 180 Mbits/s. Better yet, if each hologram had contained 1,000,000 pixels, then the recording rate would be 1 Gbits/s. So from the side of optics, high speed data storage and retrieve is not a problem. However we will need to acquire the necessary SLM, beam deflection modules, control electronics, and detector array to complete the system.

So far we have shown material characterization, component characterization, and high density recording. What we haven't shown is the complete system working in its intended capacity. The WORM system we have constructed is intended to product high density master disks which can then be mass produced and read by simple readers. In Section 4.0 we have shown that the stored data can be read out by the recorder with fair SNR. In the remainder of this section we will describe an experiment where a disk was produced by the recorder and then read by a separate reader.

Figure 5.1 shows a simple block diagram of the compact holographic disk reader. It uses a 50mW DPSS laser module to reconstruct the holograms. The beam passes through a modulator which is acting as a very fast shutter. Two galvo scanners position the reference beam on the disk and the reconstruction is imaged with the same custom designed *f*/1.1 lens used in the recorder onto the Philips CCD array for readout. During the recording process, we also recorded two independent pixels and their reconstruction fall on two separate quadrant detectors. The signals generated from these quadrant detectors are used for tracking and firing the modulator. Figure 5.2 shows a picture of the compact holographic disk reader. Its current dimensions are 17" by 10" by 9". Figure 5.3 shows a close-up picture of the disk (middle and to the right), the imaging lens (middle), and CCD array (middle and lower).

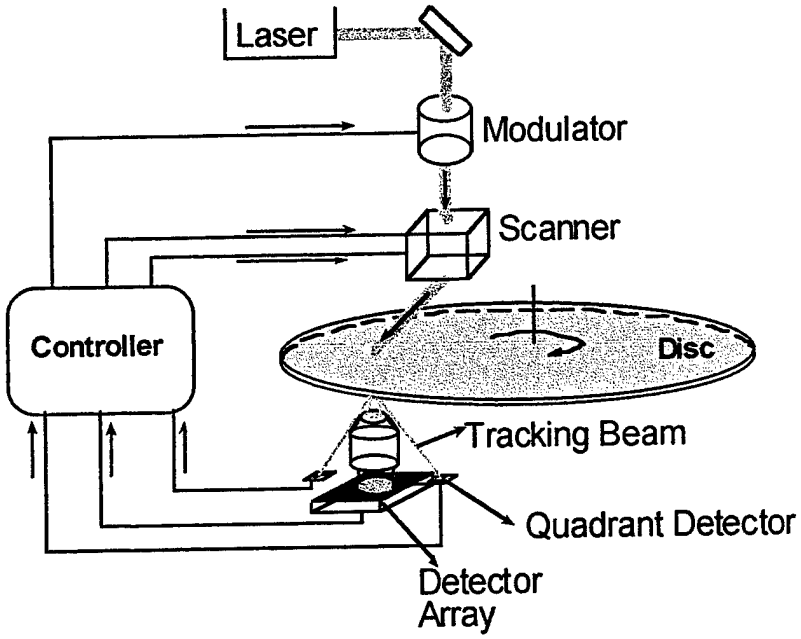

Figure 5.1: A simple block diagram of the holographic disk reader.

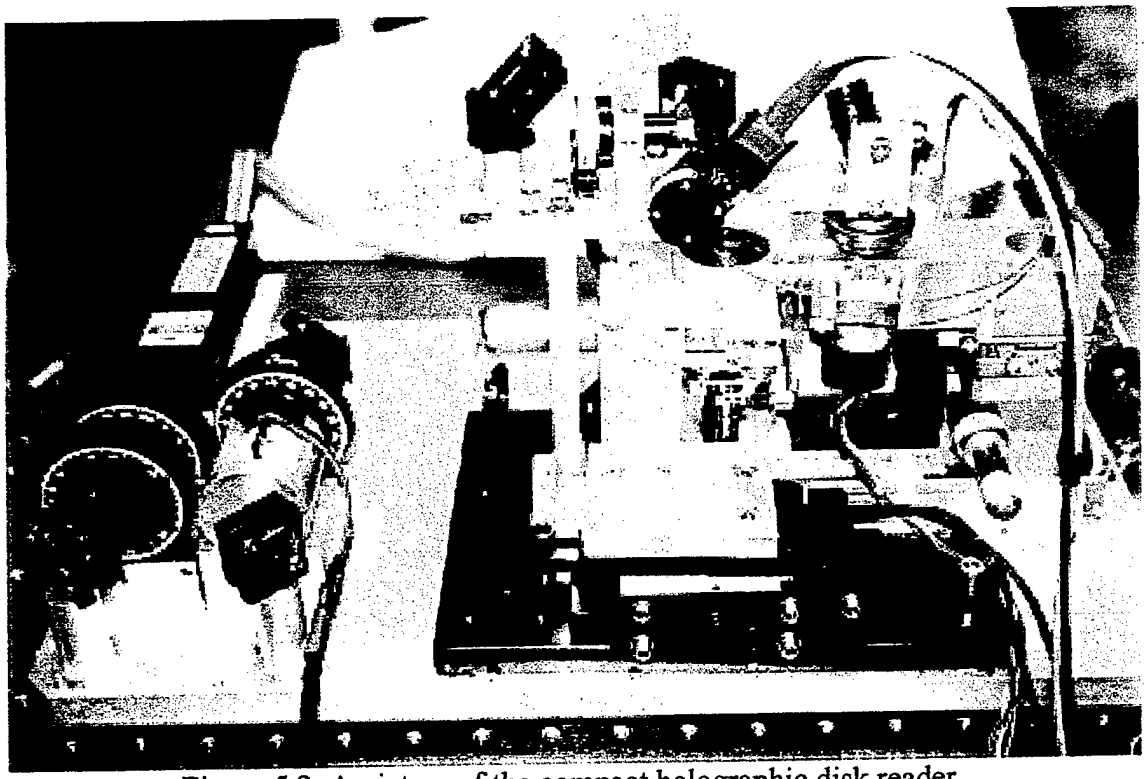

Figure 5.2: A picture of the compact holographic disk reader.

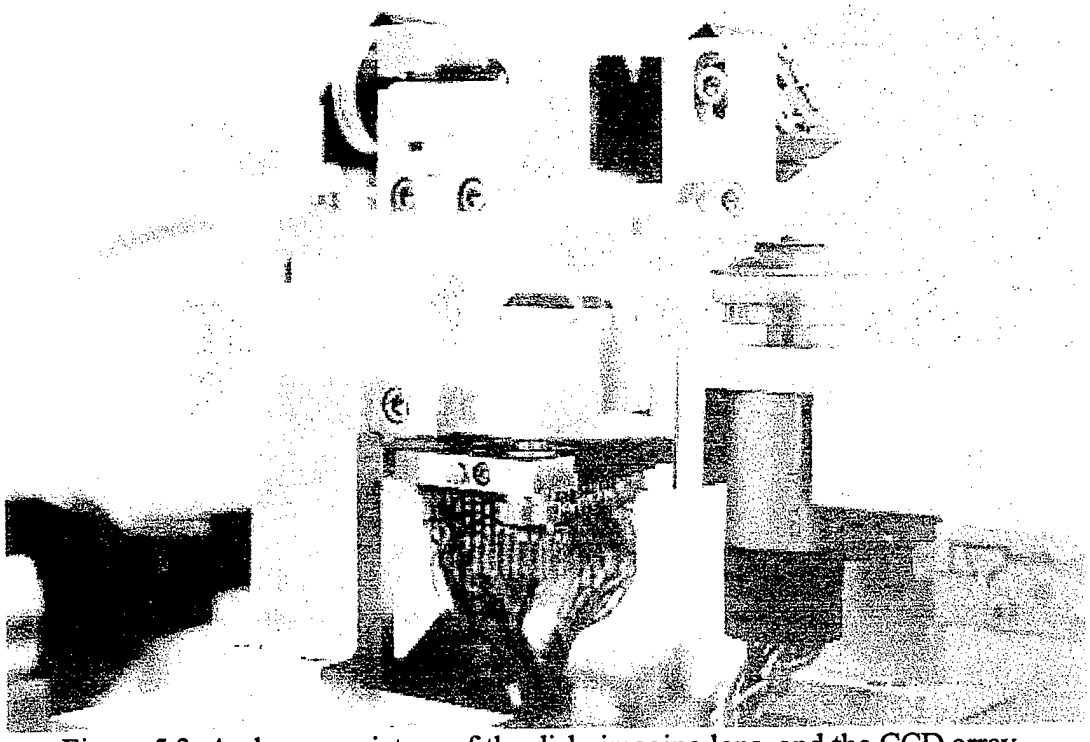

Figure 5.3: A close-up picture of the disk, imaging lens, and the CCD array.

Several images of flowers were encoded using Hamming code with a 33% overhead and then recorded onto a holographic disk with the recorder. Figure 5.4 (a) shows a portion of one such data page. The disk was then removed from the recorder and then placed in the reader for reconstruction. Using the signals generated by the two quadrant detectors, the reader was able to track the stored holograms and reconstruct the data pages. A computer then decodes the stored images (Figure 5.4 (b)). For this particular experiment, all the stored images were recalled without errors (the Hamming code was able to correct all the errors experienced). This experiment demonstrates that the compact holographic reader can read data stored with the high density recorder. The compact holographic reader setup and experiments are discussed in detail in contract C0125.

(a) (b)

Figure 5.5: (a) A portion of a data page recorded in the holographic disk, (b) the original image encoded in the data page.

MISSION
OF
AFRL/INFORMATION DIRECTORATE (IF)

The advancement and application of information systems science and technology for aerospace command and control and its transition to air, space, and ground systems to meet customer needs in the areas of Global Awareness, Dynamic Planning and Execution, and Global Information Exchange is the focus of this AFRL organization. The directorate's areas of investigation include a broad spectrum of information and fusion, communication, collaborative environment and modeling and simulation, defensive information warfare, and intelligent information systems technologies.